Journal of Asian Earth Sciences 166 (2018) 181–194

Contents lists available at ScienceDirect

Journal of Asian Earth Sciences

journal homepage: www.elsevier.com/locate/jseaes

Full length article

MgO partition between olivine and K_2O-rich silicate melt: Geothermometers applicable to high potassium magmas

Liping Liu, Xiaomin Hu, Xi Liu*

School of Earth and Space Sciences, Peking University, Beijing 100871, China
Key Laboratory of Orogenic Belts and Crustal Evolution, Ministry of Education of China, Beijing 100871, China

ARTICLE INFO

Keywords:
Geothermometer
High potassium magmas
Magma temperature
MgO partition
Olivine

ABSTRACT

Potassium and ultrapotassium magmas with potential origins in the upper mantle are common and widely distributed on the Earth. Previous experimental studies have suggested that K can significantly decrease the partial melting *T* of the peridotite. Since K has a strong effect on the melt composition, and on the molar partition coefficient of some cations such as Mg between the olivine and melt, $D_{Mg}^{Ol/liq}$, it can substantially affect the *T* estimation of the Ol geothermometers. However, none of the presently available geothermometers have critically considered the effect of K. In this paper, we have collected a large number of composition data of the Ol-melt equilibrium pairs covering a large range of K_2O contents in the melts, and have successfully calibrated three K_2O-dependent geothermometers on the basis of the MgO partition between the Ol and basaltic magma, two Ol geothermometers and one melt composition geothermometer. The database covers the *P* range from 1 atm to 7 GPa and *T* range of 1087–1950 °C. Compared to some other geothermometers, our Ol geothermometers reproduce the experimental *T* very well, with the average of the absolute differences between the calculated *T* and experimental *T* being only 14(15) °C at room *P* and 25(21) °C at high *P*, and with these differences showing no clear dependence on the *P*, *T*, and contents of K_2O and any other oxides in the melts. Furthermore, our melt composition geothermometer allows excellent *T* estimate for the silicate magma coexisting with Ol by using the melt composition alone. The application of our melt composition geothermometer to the Somma-Vesuvius volcanic complex in Italy demonstrates that this geothermometer can lead to reasonable *T* estimates for the high potassium silicate magmas, even there are small amounts of volatiles such as H_2O and CO_2 in the melts.

1. Introduction

Temperature (*T*) is one of the key physical parameters of the Earth's interior, and it can strongly affect a large number of physical and chemical properties of the Earth materials, such as density, elasticity, viscosity, electrical conductivity, seismic velocity, melting behavior, trace element partitioning, isotope fractionation, etc. Consequently, accurate estimate of *T* in the Earth's interior is critical to the interpretation of the internal structure, the geodynamic process, and the evolution of the Earth. There are several methods for the estimation of *T* in the Earth's interior, like the geothermal method (Ádám, 1978), geoelectrical method (Shankland and Ander, 1983), seismic method (Anderson, 1980) and experimental petrology (Boyd, 1973). Among them, the most common and straightforward method probably is the mineral–mineral/melt geothermometer method based on some particular chemical equilibrium among different phases at different pressure (*P*)-*T* conditions (e.g. O'Neill and Wood, 1979; Ford et al., 1983).

Basaltic magma activity is an evident indicator of the high *T* state of the Earth's upper mantle, and magma can be used to constrain the *T* (Ford et al., 1983; Beattie, 1993; Gudfinnsson and Presnall, 2001; Putirka et al., 2007; Falloon et al., 2007). As the upper mantle is ultramafic and mineralogically dominated by olivine (Ol), the basaltic magma generated in the partial melting process of the upper mantle is always buffered by Ol (Green and Ringwood, 1967; Jaques and Green, 1980). Once the magma leaves its source region, it remains in continuous chemical equilibrium with Ol for the most part of its low-*P* evolution process, due to the rapid expansion of the primary phase volume of Ol at low *P* (Presnall et al., 1978). The usefulness of the chemical equilibrium between the basaltic magma and Ol as a potential geothermometer was realized a long time ago. Since Roeder and Emslie (1970) published the first geothermometer model, there have been numerous attempts which have led to different versions of basaltic magma-Ol geothermometers (e.g. Longhi et al., 1978; Ford et al., 1983; Nielsen, 1988; Beattie, 1993; Sugawara, 2000; Gudfinnsson and Presnall, 2001; Herzberg and O'Hara, 2002; Putirka, 2005; Putirka et al., 2007).

Due to the chemical equilibrium between the Ol and basaltic magma, the partition coefficient of some cations between these two

* Corresponding author at: School of Earth and Space Sciences, Peking University, Beijing 100871, China.
E-mail address: xi.liu@pku.edu.cn (X. Liu).

https://doi.org/10.1016/j.jseaes.2018.07.036
Received 17 April 2018; Received in revised form 29 June 2018; Accepted 22 July 2018
Available online 23 July 2018
1367-9120/

phases ($D_{Mg}^{ol/liq}$ as an example; $D_{Mg}^{ol/liq} = X_{Mg}^{ol}/X_{Mg}^{liq}$, where X_{Mg}^{α} is the molar fraction of Mg in phase α) is in positive correlation with $1/T$ at constant P; or, $lnD_{Mg}^{ol/liq}$is near-linear positively correlated with $1/T$ (e.g. Roeder and Emslie, 1970; Roeder, 1974; Leeman, 1978; Ford et al., 1983). This is the theoretical basis for the so-called Ol geothermometer (Roeder and Emslie, 1970). According to Irvine and Kushiro (1976), Hart and Davis (1978) and Watson (1977), however, the cation partition coefficients between the Ol and magma are strongly dependent upon the liquid compositions. Moreover, Roeder (1974), Herzberg (1979) and Leeman (1978) observed strong effects of the alkali contents on the cation partitioning coefficients. Indeed, direct partial melting experiments of the mantle lherzolite demonstrated that both K_2O and Na_2O could strongly affect the compositions of the melt, but not the compositions of the Ol (Sack et al., 1987; Walter and Presnall, 1994; Liu and O'Neill, 2004a), leading to large variations of the cation partition coefficients, which should in turn affect the T-estimation capability of the Ol geothermometer. According to Wasylenki et al. (2003) and Liu and O'Neill (2004a), 1 wt% of K_2O in the melt decreases the solidus of the mantle lherzolite by ~7 or 5.8 °C, respectively; in comparison, 1 wt% Na_2O decreases the solidus by ~4.3 °C (Liu et al., 2006).

During the partial melting process of the upper mantle, K_2O is strongly incompatible and concentrates in the low fraction melt. As a result, potassium or ultrapotassium magmas originating from the upper mantle are common and widely distributed on the Earth, like those Plio-Quaternary magmas in central-southern Italy (Conticelli and Peccerillo, 1992) and those Cenozoic basaltic magmas in eastern China (especially in the Wudalianchi region; Zou et al., 2003). According to our statistics on 1602 Cenozoic basaltic samples (either primitive or somewhat evolved) from eastern China, their K_2O content ranges from 0.24 to 9.29 wt% (Fig. 1); in comparison, their Na_2O content varies from 0.65 to 6.96 wt% only. As revealed by Fig. 1, there is no convincing correlation between the K_2O and SiO_2, or between the K_2O and MgO, so that the variation of the K_2O contents largely reflects the partial melting process in the source mantle. It thus appears truly necessary to take into account the effect of K_2O when one uses the magma-Ol equilibrium to estimate the T of the mantle, as previously pointed out by Luth (1967), Roeder (1974), Irvine and Kushiro (1976), Leeman (1978), Herzberg (1979), and Gudfinnsson and Presnall (2001).

Due to lacking experimental data, however, the influence of K_2O on the partitioning of Mg and other cations between the basaltic magma and Ol has never been critically evaluated. Schairer (1954) reported some preliminary experimental data in the system MgO-Al_2O_3-SiO_2-K_2O (MASK) at 1 atm. Recently, Conceição and Green (2000) conducted experiments to investigate the enstatite-Ol cotectic curve in the system MgO-Al_2O_3-SiO_2-K_2O-FeO (MASKF) at 0.5–2.0 GPa whereas Liu and O'Neill (2004a, 2004b) investigated the partial melting process of spinel lherzolite in the systems CaO-MgO-Al_2O_3-SiO_2-K_2O (CMASK) and CaO-MgO-Cr_2O_3-Al_2O_3-SiO_2-K_2O (CMCrASK) at 1.1 GPa. As to the 1 atm condition, Hu (2011) lately reported in her master-degree thesis 46 composition pairs of coexisting Ol and melt in the system CMASK. Furthermore, Davis and Hirschmann (2013) and Laporte et al. (2014) deliberately added K_2O to their natural peridotitic starting materials, carried out partial melting experiments from 1.0 to 3.0 GPa, and obtained some compositional data of K_2O-rich melts in equilibrium with Ol. Now it seems appropriate to assess the effects of K_2O on the cation partitioning between the basaltic magma and Ol. In this paper, we have calibrated three K_2O-dependent geothermometers on the basis of the MgO partition behavior between the basaltic magma and Ol, verified it with some experimental data which were not used in the calibration, and applied it to those K_2O-rich Plio-Quaternary magmas in central-southern Italy.

2. Preparing the database

So far, a large number of compositional data of the Ol-melt equilibrium pairs experimentally-obtained under various P-T conditions have been published, and some databases compiling these compositional data, like the LEPR database (http://lepr.ofm-research.org), exist. However, the K_2O concentrations of the melts included in these databases are usually very low.

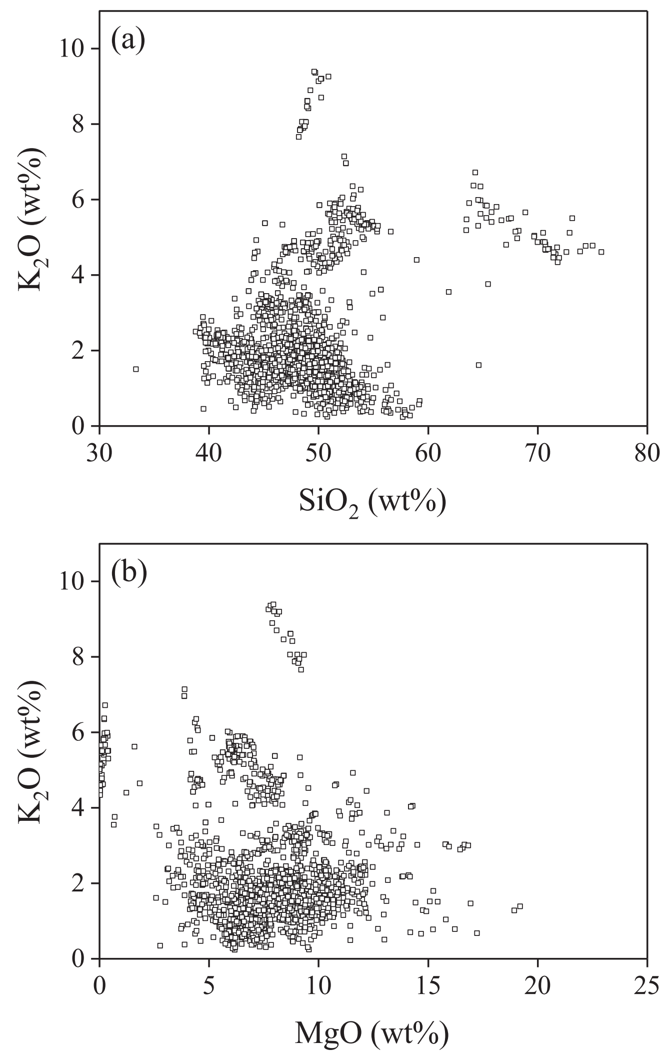

Fig. 1. K_2O vs SiO_2 (a) and K_2O vs MgO (b) of Cenozoic igneous rocks with mantle origin from east China (1602 whole-rock composition data). The content of K_2O is between 0.24 and 9.29 wt%. Note that some of the igneous rocks were severely affected by Pl (plus other phases) crystallization at low P, as indicated by their > ~60% SiO_2 contents (Liu et al., 2015). Data Source: Basu et al. (1991), Fan and Hooper (1991), Zhang et al. (1991), Liu et al. (1992), Zhou et al. (1992), Liu et al. (1994), Qi et al. (1994), Chung et al. (1995), Zhang et al. (1995), Zhi et al. (1995), Cong et al. (1996), Chung et al. (1997), Fan et al. (1998), Hsu and Chen (1998), Yang et al. (1998), Chung (1999), Fan et al. (1999), Han et al. (1999), Ho et al. (2000), Hsu et al. (2000), Zhang et al. (2000), Zou et al. (2000), Cong et al. (2001), Zhang et al. (2002), Chen et al. (2003), Ho et al. (2003), Zou et al. (2003), Xu et al. (2004), Wu et al. (2005), Xu et al. (2005), Zhang et al. (2005), Fan et al. (2006a), Fan et al. (2006b), Guo et al. (2006), Lee et al. (2006), Tang et al. (2006), Zhang and Han (2006), Chen et al. (2007), Chuvashova et al. (2007), Fan et al. (2007), Yan et al. (2007), Chen et al. (2008), Ho et al. (2008), Liu et al. (2008), Yan and Zhao (2008), Zou et al. (2008), Chen et al. (2009), Kuritani et al. (2009), Luo et al. (2009), Zhang et al. (2009), Zeng et al. (2010), Ho et al. (2011), Kuritani et al. (2011), Rasskazov et al. (2011), Wang et al. (2011), Zeng et al. (2011), Xu et al. (2012a), Xu et al. (2012b), Chu et al. (2013), Ho et al. (2013), Hong et al. (2013), Kuritani et al. (2013), Lee et al. (2013), Sakuyama et al. (2013), Zeng et al. (2013), Li et al. (2014), Sun et al. (2014), Zhao et al. (2014), Chen et al. (2015), Huang et al. (2015), Yu et al. (2015a), Yu et al. (2015b), Li et al. (2016a), Li et al. (2016b), Zeng et al. (2016), Li et al. (2017), Liu et al. (2017), Wang et al. (2017).

For the purpose of calibrating a K_2O-dependent geothermometer, a database with its melt compositions covering a wide range of K_2O contents is a prerequisite. We have scrutinized the literature and collected the composition data of the Ol-melt equilibrium pairs which show a large range of K_2O contents in the melts. Our data have been divided into three groups: (1) Group 1 includes the data from some simple systems such as the CMASK, MASKF and CMCrASK; (2) Group 2 includes the data from the natural composition system at 1 atm; (3) Group 3 includes the data from the natural composition system at high *P*.

Group 1: Compositional data of Ol-melt pairs from simple systems. In total, we have collected compositional data for 96 Ol-melt pairs from the partial melting experiments conducted in some K-bearing simple systems (STable 1): 25 data from the MASKF system at 0.5–2.0 GPa (Conceição and Green, 2000), 9 data from the CMASK system at 1.1 GPa (Liu and O'Neill, 2004a), 17 data from the CMCrASK system at 1.1 GPa (Liu and O'Neill, 2004b), and 45 data from the CMASK system at 1 atm (Hu, 2011). This group of data covers a *P* range of 1 atm - 2.0 GPa, a *T* range of 1150–1400 °C, and a K_2O range in the melt phase of 0.47–16.2 wt% (Fig. 2a).

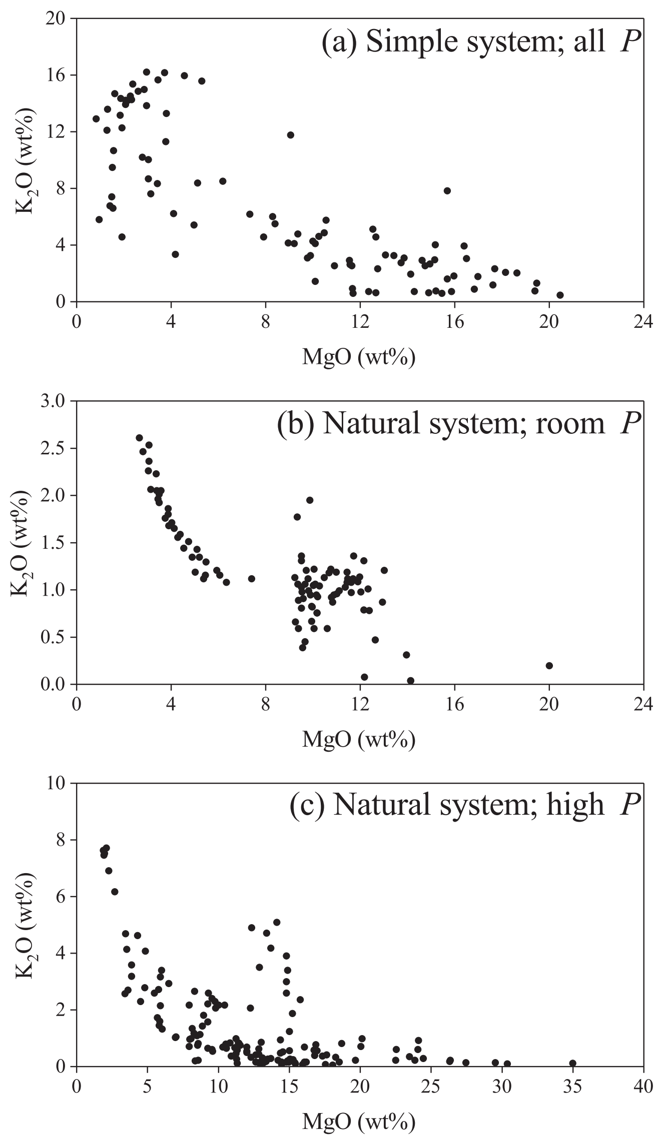

Fig. 2. K_2O vs. MgO (wt%) of some experimental melts coexisting with various Ol-bearing solid phase assemblages: (a) data from simple systems CMASK (Liu and O'Neill, 2004a; Hu, 2011), CMCrASK (Liu and O'Neill, 2004b), and MASKF (Conceição and Green, 2000), as listed in STable 1; (b) data from natural rock compositions at 1 atm (Ford et al., 1983; Grove and Juster, 1989; see STable 2 for the details); (c) data from high-*P* partial melting experiments with complex peridotitic compositions and crystallization experiments with complex rock compositions (Draper and Johnston, 1992; Kushiro, 1996; Draper and Green, 1997; Kinzler, 1997; Walter, 1998; Draper and Green, 1999; Schwab and Johnston, 2001; Laporte et al., 2004; Davis and Hirschmann, 2013; Laporte et al., 2014; see STable 3 for the details).

Supplementary data associated with this article can be found, in the online version, at https://doi.org/10.1016/j.jseaes.2018.07.036.

The data from Hu (2011) have not been published elsewhere. The experiments in Hu (2011) were conducted with a vertical high-*T* furnace installed at the High-Pressure Laboratory of Peking University; the *T* distribution around the hot spot in this furnace was accurately mapped with a $Pt_{94}Rh_6$-$Pt_{70}Rh_{30}$ thermocouple, and the uncertainty in the *T* measurements should be less than 5 °C. The experimental materials were encapsulated in Pt capsules arc-welded at both ends, so that severe K_2O-losing at high *T* was avoided. The experimental charges were quickly quenched in cold water after running for desired amounts of time (Table 1), and the experimental products were processed for later scanning electron microscopy and electronic microprobe analysis (JEOL JXA8100). In total, Hu (2011) documented compositional data for 46 Ol-melt pairs, covering the *T* range of 1150–1400 °C; the K_2O content in the melt phase ranged from 0.47 to 10.64 wt% (Table 1). With the exception of the compositional data for one Ol-melt pair only (HXL048; Hu, 2011), all other data are of high quality. Hu (2011) also analyzed for the compositions of other phases (orthopyroxene, clinopyroxene and plagioclase) coexisting with the Ol and melt; the results will be fully reported somewhere else.

Schairer (1954) reported some phase equilibrium data in the system MASK at 1 atm, without fully quantifying the melt composition. Since there was potential alkali-loss problem, extracting compositional data from his phase diagram would lead to large uncertainty. Consequently, his data are excluded from our database.

Group 2: Compositional data of Ol-melt pairs from natural composition system at 1 atm. In total, we have collected compositional data for 100 Ol-melt pairs experimentally-obtained using natural compositions at 1 atm (STable 2): 67 data from Ford et al. (1983) and 33 data from Grove and Juster (1989). The experiments of Ford et al. (1983) determined the cation partition between the Ol and basic/ultrabasic magma at controlled oxygen fugacity ranging from $10^{-5.08}$ to $10^{-11.5}$ bars (Falloon et al., 2007). Grove and Juster (1989) supplied compositional data between the Ol and basaltic/andesitic magma at controlled oxygen fugacity ranging from $10^{-5.93}$ to $10^{-9.89}$ bars. The experiments from these two studies covered the *T* range of 1087–1446 °C (STable 2), and the K_2O, Na_2O and MgO contents of the melts ranged from 0.04 to 2.61 wt%, from 0.06 to 4.48 wt% and from 2.66 to 20 wt%, respectively (Fig. 2b). As to the charge state of iron, our calculation using the method of Kress and Carmichael (1988) suggests that the $Fe^{3+}/(Fe^{2+}+Fe^{3+})$ ratios in the melts from Ford et al. (1983) and Grove and Juster (1989) are from 0.02 to 0.30 and from 0.11 to 0.42, respectively.

Group 3: Compositional data of Ol-melt pairs from natural composition system at high P. In total, we have collected compositional data for 142 Ol-melt pairs experimentally-obtained using natural compositions at high *P* (STable 3). The data sources are Kushiro (1996), Kinzler (1997), Walter (1998), Schwab and Johnston (2001), Laporte et al. (2004), Davis and Hirschmann (2013) and Laporte et al. (2014) which are experimental studies of partial melting process of mantle peridotites, and Draper and Johnston (1992) and Draper and Green (1997; 1999) which are experimental studies of crystallization process of high-MgO basalt and silicic-alkaline-aluminous melts, respectively. This group of data covers a *P* range of 0.5–7.0 GPa, a *T* range of 1115–1950 °C, a Na_2O range in the melts of 0.28–7.24 wt% and a K_2O range in the melts of 0.06–7.5 wt% (Fig. 2c). All the experiments in these studies cited here were done using graphite capsule with/without large platinum outer capsule; according to Médard et al. (2008), the amount of Fe^{3+} is negligible ($Fe^{3+}/(Fe^{2+}+Fe^{3+}) < 0.05$) and would not significantly affect thermodynamic properties. Additionally, there are several issues to be mentioned: firstly, Kushiro (1996) did not report the Ol composition; secondly, the melts in four experiments of Laporte et al. (2004) contained some water (0.28–1.13 wt%); thirdly, Laporte et al. (2014) did not report the Ol composition and their melts contained some water (0.02–1.15 wt%).

Overall, the database (Group 1, Group 2 and Group 3) assembled in

Table 1
Experimental conditions, phase assemblages, and compositions of Ol and melt.

		SiO_2	MgO	CaO	Al_2O_3	K_2O
HXL037, 1400 °C[a]	Ol (9)[b]	42.91(17)[c]	56.75(16)	0.28(2)	0.05(2)	0.01(1)
Ol + Melt	Melt (7)	54.75(19)	19.40(21)	12.73(6)	12.37(7)	0.75(3)
HXL038, 1400 °C	Ol (10)	42.81(15)	56.79(14)	0.35(2)	0.04(1)	0.01(1)
Ol + Melt	Melt (9)	54.18(15)	17.70(21)	13.18(26)	12.64(13)	2.30(6)
HXL039, 1400 °C	Ol (10)	42.61(22)	56.90(22)	0.43(1)	0.04(2)	0.01(1)
Ol + Melt	Melt (10)	53.82(21)	16.39(22)	13.05(20)	12.80(13)	3.94(13)
HXL040, 1400 °C	Ol (8)	42.88(16)	56.81(14)	0.28(2)	0.03(2)	–
Ol + Opx + Melt	Melt (9)	59.18(19)	20.47(14)	11.41(5)	8.46(9)	0.47(3)
HXL041, 1400 °C	Ol (10)	42.96(15)	56.76(15)	0.26(1)	0.02(2)	0.01(1)
Ol + Opx + Melt	Melt (9)	60.41(11)	19.47(16)	10.86(15)	7.94(11)	1.32(5)
HXL042, 1400 °C	Ol (10)	42.76(23)	56.95(24)	0.26(2)	0.02(1)	0.01(2)
Ol + Opx + Melt	Melt (10)	61.46(21)	18.63(20)	10.41(8)	7.48(10)	2.02(11)
HXL010, 1350 °C	Ol (10)	42.25(17)	57.44(18)	0.28(2)	0.04(2)	–
Ol + Melt	Melt (7)	55.37(23)	15.86(10)	14.04(5)	14.00(26)	0.73(2)
HXL011, 1350 °C	Ol (10)	42.41(14)	57.16(16)	0.37(3)	0.04(2)	0.01(1)
Ol + Melt	Melt (10)	54.13(25)	14.94(11)	14.08(16)	14.20(15)	2.65(9)
HXL012, 1350 °C	Ol (10)	42.39(16)	57.10(15)	0.48(3)	0.03(2)	0.01(1)
Ol + Melt	Melt (8)	53.92(14)	12.66(17)	14.48(16)	14.36(12)	4.58(7)
HXL013, 1350 °C	Ol (10)	42.48(15)	57.16(16)	0.34(3)	0.02(2)	–
Ol + Opx + Melt	Melt (10)	58.19(21)	15.20(24)	13.93(7)	11.93(8)	0.75(3)
HXL014, 1350 °C	Ol (9)	42.44(10)	57.20(10)	0.34(2)	0.02(1)	–
Ol + Opx + Melt	Melt (8)	59.83(19)	14.15(14)	13.07(8)	11.01(8)	1.94(10)
HXL015, 1350 °C	Ol (9)	42.57(20)	57.00(20)	0.39(2)	0.02(2)	0.02(1)
Ol + Melt	Melt (10)	60.40(18)	13.07(13)	12.61(7)	10.65(18)	3.27(7)
HXL017, 1350 °C	Ol (10)	42.20(20)	57.30(20)	0.44(2)	0.04(3)	0.02(1)
Ol + Melt	Melt (9)	54.48(10)	13.73(8)	14.52(10)	14.52(13)	2.74(9)
HXL018, 1350 °C	Ol (9)	42.16(19)	57.17(21)	0.64(3)	0.02(2)	0.01(1)
Ol + Cpx + Melt	Melt (10)	54.82(14)	14.62(17)	17.41(22)	10.23(15)	2.91(8)
HXL001, 1300 °C	Ol (10)	42.47(19)	57.15(18)	0.34(2)	0.04(2)	0.01(1)
Ol + Melt	Melt (8)	56.57(26)	12.36(14)	15.29(13)	15.07(15)	0.71(2)
HXL002, 1300 °C	Ol (10)	42.54(17)	56.99(18)	0.45(2)	0.03(1)	–
Ol + Melt	Melt (8)	55.01(19)	11.55(13)	15.35(7)	15.18(13)	2.92(10)
HXL003, 1300 °C	Ol (7)	42.65(6)	56.75(6)	0.56(4)	0.03(2)	0.01(1)
Ol + Melt	Melt (9)	54.80(28)	10.49(17)	14.96(11)	14.91(20)	4.84(9)
HXL004, 1300 °C	Ol (10)	42.53(26)	57.05(25)	0.37(3)	0.05(2)	0.01(1)
Ol + Opx + Cpx + Melt	Melt (10)	57.72(20)	12.66(12)	15.29(12)	13.71(27)	0.63(2)
HXL005, 1300 °C	Ol (7)	42.66(9)	56.91(12)	0.37(3)	0.05(3)	–
Ol + Opx + Cpx + Melt	Melt (9)	59.85(12)	10.92(13)	13.21(7)	13.51(11)	2.51(8)
HXL006, 1300 °C	Ol (8)	42.56(13)	57.02(16)	0.37(6)	0.03(2)	0.02(1)
Ol + Cpx + Melt	Melt (9)	62.32(16)	8.96(14)	11.08(6)	13.49(10)	4.15(8)
HXL008, 1300 °C	Ol (9)	42.57(16)	56.89(15)	0.50(2)	0.03(2)	0.01(1)
Ol + Cpx + Melt	Melt (9)	55.22(26)	11.65(17)	15.87(9)	14.74(13)	2.53(10)
HXL009, 1300 °C	Ol (10)	42.41(25)	56.96(27)	0.57(2)	0.04(2)	0.02(1)
Ol + Cpx + Melt	Melt (8)	54.94(14)	10.26(12)	14.81(10)	15.40(9)	4.59(5)
HXL019, 1260 °C	Ol (9)	42.74(11)	56.90(11)	0.29(4)	0.06(2)	0.01(1)
Ol + Cpx + Melt	Melt (9)	56.14(17)	11.68(15)	15.46(17)	15.80(10)	0.92(4)
HXL020, 1260 °C	Ol (10)	42.45(13)	57.09(14)	0.41(3)	0.04(2)	0.01(1)
Ol + Cpx + Melt	Melt (9)	55.13(14)	9.89(12)	14.58(12)	17.16(14)	3.24(11)
HXL021, 1260 °C	Ol (8)	42.51(5)	56.94(7)	0.48(2)	0.05(3)	0.01(1)
Ol + Cpx + Melt	Melt (10)	54.23(29)	8.30(23)	13.39(17)	18.06(14)	6.02(12)
HXL022, 1260 °C	Ol (10)	42.60(24)	57.14(25)	0.23(3)	0.03(1)	–
Ol + Opx + Cpx + Melt	Melt (9)	56.88(22)	11.70(27)	15.07(15)	15.75(15)	0.60(3)
HXL023, 1260 °C	Ol (10)	42.57(22)	57.20(22)	0.18(2)	0.03(2)	0.01(1)
Ol + Opx + Cpx + Melt	Melt (10)	60.46(25)	10.09(16)	12.87(11)	15.13(15)	1.44(5)
HXL024, 1260 °C	Ol (9)	42.59(7)	57.17(7)	0.21(2)	0.02(2)	0.01(1)
Ol + Cpx + Melt	Melt (10)	62.39(21)	7.92(11)	10.47(12)	14.65(17)	4.57(10)
HXL026, 1260 °C	Ol (9)	42.68(12)	56.82(11)	0.47(3)	0.02(2)	0.01(1)
Ol + Cpx + Melt	Melt (8)	55.42(12)	9.78(13)	14.70(15)	17.04(13)	3.06(8)
HXL027, 1260 °C	Ol (11)	42.61(13)	56.85(12)	0.50(3)	0.03(2)	0.01(1)
Ol + Cpx + Melt	Melt (9)	54.87(18)	8.41(12)	13.54(16)	17.70(15)	5.48(9)
HXL028, 1200 °C	Ol (10)	42.85(24)	56.86(24)	0.25(2)	0.03(2)	0.01(1)
Ol + Opx + Cpx + Pl + Melt	Melt (10)	67.25(1 1 1)	4.11(33)	7.06(41)	15.36(52)	6.21(57)
HXL029, 1200 °C	Ol (8)	42.87(5)	56.80(9)	0.28(3)	0.05(3)	0.02(1)
Ol + Cpx + Pl + Melt	Melt (8)	65.92(20)	3.42(6)	5.92(9)	16.42(12)	8.33(21)
HXL030, 1200 °C	Ol (8)	42.90(10)	56.70(9)	0.35(3)	0.03(3)	0.02(1)
Ol + Cpx + Pl + Melt	Melt (9)	63.87(12)	3.03(6)	5.63(15)	17.46(20)	10.01(12)
HXL031, 1200 °C	Ol (10)	43.06(22)	56.61(23)	0.28(4)	0.04(2)	0.01(1)
Ol + Opx + Cpx + Pl + Melt	Melt (8)	70.54(17)	4.18(7)	8.42(9)	13.52(20)	3.34(5)
HXL032, 1200 °C	Ol (10)	43.07(12)	56.61(10)	0.28(2)	0.02(3)	0.01(1)
Ol + Opx + Cpx + Pl + Melt	Melt (9)	67.89(53)	3.14(18)	5.76(19)	15.61(25)	7.60(15)
HXL033, 1200 °C	Ol (10)	42.88(17)	56.79(15)	0.28(2)	0.05(2)	0.02(2)
Ol + Opx + Cpx + Pl + Melt	Melt (8)	63.90(8)	4.97(12)	8.58(8)	17.16(12)	5.40(11)

(*continued on next page*)

Table 1 (*continued*)

		SiO_2	MgO	CaO	Al_2O_3	K_2O
HXL035, 1200 °C	Ol (10)	43.16(13)	56.49(10)	0.30(2)	0.03(2)	0.02(2)
Ol + Cpx + Pl + Melt	Melt (10)	67.02(21)	3.03(10)	5.31(8)	15.97(19)	8.67(10)
HXL036, 1200 °C	Ol (10)	42.75(22)	56.77(32)	0.41(15)	0.04(2)	0.03(2)
Ol + Cpx + Pl + Melt	Melt (9)	64.43(22)	2.79(9)	5.21(17)	17.39(7)	10.18(12)
HXL046, 1150 °C	Ol (9)	42.64(11)	57.03(12)	0.27(4)	0.06(2)	0.01(1)
Ol + Cpx + Pl + Melt	Melt (8)	77.53(33)	0.97(3)	3.32(9)	12.38(35)	5.80(41)
HXL047, 1150 °C	Ol (9)	42.50(8)	57.13(10)	0.31(5)	0.05(2)	0.01(1)
Ol + Cpx + Pl + Melt	Melt (8)	70.04(32)	1.53(12)	3.13(19)	15.82(12)	9.48(22)
HXL049, 1150 °C	Ol (5)	42.38(29)	57.25(29)	0.24(3)	0.12(7)	0.01(1)
Ol + Opx + Cpx + Pl + Melt	Melt (9)	76.88(49)	1.93(16)	4.77(32)	11.85(20)	4.58(18)
HXL050, 1150 °C	Ol (9)	42.54(19)	57.15(18)	0.24(3)	0.05(3)	0.02(1)
Ol + Opx + Cpx + Pl + Melt	Melt (8)	74.34(83)	1.42(6)	3.06(7)	14.39(17)	6.78(83)
HXL051, 1150 °C	Ol (9)	42.58(16)	57.13(18)	0.23(5)	0.04(3)	0.02(1)
Ol + Opx + Cpx + Pl + Melt	Melt (9)	73.44(51)	1.49(13)	3.12(18)	14.56(28)	7.39(74)
HXL053, 1150 °C	Ol (9)	42.64(18)	57.00(19)	0.29(3)	0.06(2)	0.02(2)
Ol + Cpx + Pl + Melt	Melt (9)	72.91(27)	1.55(7)	3.11(9)	15.86(18)	6.58(11)
HXL054, 1150 °C	Ol (10)	42.24(22)	57.31(22)	0.38(4)	0.03(2)	0.03(2)
Ol + Cpx + Pl + Melt	Melt (9)	66.07(1 0 7)	1.57(20)	3.02(6)	18.70(38)	10.64(1 1 6)

[a] Information listed is run number, experimental temperature, and phase assemblage where Ol is olivine, Opx is orthopyroxene, Cpx is clinopyroxene, and Pl is plagioclase. All experiments were conducted at 1 atm.

[b] Number in the parenthesis after the name of the phase is the number of successful EPM analyses performed on that phase.

[c] Numbers in the parentheses are analytical uncertainties reported as one standard deviation. 42.91(17) read as 42.91 ± 0.17.

this study contains the composition data for 295 Ol-melt pairs, and for 43 melts (Kushiro, 1996; Laporte et al., 2014). The database includes melts with compositions varying from komatiitic to rhyolitic (SiO_2: 38.31–77.53 wt%), covers a T range from 1087 to 1950 °C and a P range from 1 atm to 7 GPa. Evidently in Fig. 2, the database suggests that a general negative correlation exists between the K_2O and MgO in the melts. On one hand, we could attribute it to the incompatibility of K and an increasing melt fraction. On the other hand, this negative relationship might imply that K_2O suppresses the MgO content of the melts and has a significant effect on the $D_{Mg}^{ol/liq}$, corresponding with the results obtained in the simple system CMASK (Liu and O'Neill, 2004a). Uncertainties in the database include estimates of FeO and Fe_2O_3 contents in the melts (errors inevitable but presumably small), unquantified water contaminations which concentrated in the melts (potentially important but unsolvable without more accurate measurements; Liu et al., 2006); these uncertainties are generally negligible, as we will find out later.

The database has been divided into two parts: Part 1 will be used to calibrate our geothermometer, and Part 2 will be used to examine the calibration. All the data from Kushiro (1996) and Laporte et al. (2014), without the Ol composition reported, have been assigned to Part 2. In addition, the four data with hydrous melts from Laporte et al. (2004) and all the data in the system CMCrASK from Liu and O'Neill (2004b) are included in Part 2 and used for testing our geothermometer only. All the data from other experimental studies are arbitrarily assigned to Part 1 and Part 2 on an approximately 50–50 basis, resulting in 140 data in Part 1 and 198 data in Part 2 (with 60 data points from Kushiro (1996), Liu and O'Neill (2004b) and Laporte et al. (2014)).

3. Calibrating the Ol geothermometers

The equilibrium constant between any two phases can be expressed as

$$lnK = \frac{-\Delta G}{RT} - \frac{(P-P_0)\Delta V}{RT} = \frac{-\Delta H}{RT} + \frac{\Delta S}{R} - \frac{(P-P_0)\Delta V}{RT}, \tag{1}$$

where K is the equilibrium constant relating the activities of the corresponding components in the two phases, T is temperature in Kelvin, P is pressure in GPa, R is the gas constant, and ΔG, ΔH, ΔS, and ΔV are the changes of the Gibbs free energy, enthalpy, entropy, and volume of the reaction, respectively. The equilibrium constant between Ol and silicate melt can also be expressed as

$$K = \frac{a_{M_2SiO_4}^{liq}}{a_{M_2SiO_4}^{ol}}, \tag{2}$$

where a_M^{α} is the activity of component M in phase α. As the Ol solid solutions mix almost ideally (Birle et al., 1968; Wiser and Wood, 1991), the activity of the Ol components, Mg_2SiO_4 for example, can be approximated as

$$a_{Mg_2SiO_4}^{ol} = 1.5X_{Mg}^{ol}, \tag{3}$$

where X_{Mg}^{ol} is the molar fraction of Mg in Ol. Component activities in the melt phase, however, are difficult to determine from the melt compositions because there are no distinctive sites but cations dispersed in a matrix of silicate polymer units (Fraser, 1977; Ford et al., 1983). Different activity-composition approximations, either based on thermodynamic principles or merely empirical, have been proposed for silicate melts and partially successful in general (e.g. Leeman, 1978; Ford et al., 1983; Beattie, 1993). The empirical expression developed by Ford et al. (1983), with the capability to include additional components and handle further complicated interactions between these components in the melts, has been demonstrated to better reproduce the Ol-melt equilibrium (Falloon et al., 2007), and thus followed in this study. According to Ford et al. (1983), the activity of the Mg_2SiO_4 end-member component in the melts, $a_{Mg_2SiO_4}^{liq}$, can be expressed as

$$a_{Mg_2SiO_4}^{liq} = 1.5X_{Mg}^{liq}\left(1.5\left(X_{Mg}^{liq} + X_{Fe^{2+}}^{liq} + X_{Ca}^{liq} + X_{Mn}^{liq} + X_{Ni}^{liq}\right)\right)(3X_{Si}^{liq}) \tag{4}$$

where X_i^{liq} represents the molar fraction of i in the melts. Combining these equations, we obtain

$$\begin{aligned} lnD_{Mg}^{Ol/liq} = {} & C_0 + \frac{C_1}{T} + C_2\frac{P}{T} \\ & + C_3ln(1.5(X_{Mg}^{liq} + X_{Fe^{2+}}^{liq} + X_{Ca}^{liq} + X_{Mn}^{liq} + X_{Ni}^{liq})) + C_4ln(3X_{Si}^{liq}) \\ & + C_5ln(1-X_{Na}^{liq}) + C_6ln(1-X_K^{liq}) + C_7ln(1-X_{Al}^{liq}) \\ & + C_8ln(1-X_{Fe^{3+}}^{liq}) + C_9ln(1-X_{Ca}^{liq}) + C_{10}ln(1-X_P^{liq}) \\ & + C_{11}ln(1-X_{Ti}^{liq}) + C_{12}ln(1-X_{Cr^{3+}}^{liq}) \end{aligned} \tag{5}$$

where constants C_i are regression coefficients derived by a least-squares multiple linear regression, with C_0, C_1, and C_2 representing $\frac{\Delta S}{R}$, $\frac{P_0\Delta V-\Delta H}{R}$ and -$\frac{\Delta V}{R}$, respectively. C_0, C_1, and C_2 are calibrated on the constraint that the derived Ol geothermometer should reproduce $lnD_{Mg}^{Ol/liq}$ as accurately as possible, and their values are fixed in our model since ΔH, ΔS and ΔV are expected to be almost constant over our relatively small P, T and compositional ranges. C_3 and C_4 would attain a numerical value of -1 if the oxide components in the melts mix ideally. The last eight items in Eq. (5) represent the effects of additional components on the $lnD_{Mg}^{Ol/liq}$. Here we emphasize the difference of K and Na; since they have different impacts on the $D_{Mg}^{Ol/liq}$, melt composition, and solidus T, it would be better to treat them separately. In addition, as TiO_2 and P_2O_5 have effects on the melt composition opposite to those of the alkalis (Hirschmann et al., 1998), they are independently treated in Eq. (5) as well. As revealed by Liu and O'Neill (2004b), further, Cr^{3+} tends to substitute for the octahedrally-coordinated Al in the upper-mantle minerals (such as spinel and pyroxenes) and reduce the activity of Al_2O_3, which consequently leads to a significantly-reduced Al_2O_3 content and an enormously-increased MgO content in the coexisting melts. Our model thus takes into consideration the effect of Cr^{3+}.

Our Ol geothermometer is based on thermodynamic relationships, with empirical parameters added to improve its precision. 140 experimental data from the Part 1 of our database are used to derive the regression coefficients in Eq. (5), covering a P range of 0.0001–7.0 GPa, a T range of 1087–1950 °C. The range of the melt compositions is summarized in Table 2. The regression coefficients for Eq. (5), their standard errors, correlation coefficient (r), and standard deviations in $lnD_{Mg}^{Ol/liq}$ are presented in Table 3. The correlation coefficient (0.9933) and standard deviation (0.0833) indicate a good regression. Furthermore, we use the 69 1-atm experimental data in the Part 1 of our database to derive an Ol geothermometer especially for room P. The experimental data cover a T range from 1087 to 1400 °C; the range of the melt compositions is summarized in Table 2 as well. The obtained regression coefficients are similarly presented in Table 3. As expected, our room-P Ol geothermometer fits the experimental data better than our high P model does (Table 3), and is thus recommended in estimating the magma T when the P is known as close to 1 atm.

4. Evaluating the Ol geothermometers and comparison

Excluding the melt compositions (in total 60 data) from Kushiro (1996; no Ol composition reported), Laporte et al. (2014; no Ol composition reported), and Liu and O'Neill (2004b), the rest 138 experimental data in the Part 2 of our database are adopted to test the accuracies of our Ol geothermometers. These data cover the P range of 0.0001–7.0 GPa, T range of 1115–1835 °C and K_2O range of 0.04–16.2 wt%. High-P experimental data (0.5–7 GPa) have been used to examine our high-P Ol geothermometer whereas 1 atm experimental data have been used in the testing of our room-P Ol geothermometer. Testing results are presented in Figs. 3, 4 and Table 4.

As revealed by Fig. 3a, our room-P Ol geothermometer reproduces the experimental T (T_{exp}) very well: most data points of the calculated T (T_{cal}) versus T_{exp} are distributed along the 1:1 line and within a deviation of ± 50 °C, with the exception of two data points from Hu (2011; HXL049 and HXL031) at 1150 and 1200 °C, which might be due to some disequilibrium at these relatively low T. The average of the absolute differences between the T_{cal} and T_{exp} is only 14(15) °C (Table 4). As shown in Fig. 3b, our high-P Ol geothermometer also reproduces the high-P T_{exp} (0.5–7 GPa) very well, with a few data points falling out of the ± 50 °C deviation lines. The average of the absolute differences between the T_{cal} and T_{exp} is only 25(21) °C (Table 4).

The capability of our Ol geothermometers handling the K_2O has been tested. Ideally, the differences between T_{cal} and T_{exp} should not define any clear dependence on the K_2O contents in the melts. The results of our examination (Fig. 4a and 4d) meet this expectation. Putirka et al. (2007) also developed an empirical expression which was supposed to account for the effect of K_2O (their Eq. (2); termed as P2007-(2)); note their assumption of identical effects of K_2O and Na_2O. Our tests however show that P2007-(2) actually could not accurately reproduce the experimental data: as shown in Fig. 4b and 4e, obvious positive correlations between the $T_{exp} - T_{cal}$ and K_2O content exist. With the addition of some extra terms, Putirka et al. (2007) recalibrated Eq. (10) of Beattie (1993) and arrived at another geothermometer, their Eq. (4) (P2007-(4) hereafter), which essentially ignored the influence of K_2O. For the purpose of comparison, we have tested the performance of P2007-(4) as well: the results show, surprisingly, that P2007-(4) reproduces the T_{exp} much better than P2007-(2) (Fig. 4c and 4f), especially at high-P conditions. Nevertheless, a clear dependence of the $T_{exp} - T_{cal}$ on the K_2O contents in the melts has been defined for P2007-(4), especially for the room P condition (Fig. 4c).

The capability of our Ol geothermometers handling other compositional variables, P and T has been tested similarly (with figures nonshown). With the exceptions of FeO and P_2O_5, all other variables can be successfully processed by our high-P Ol geothermometer, as indicated by the small R^2 values (typically < ~0.1) for the linear regressions between the $T_{exp} - T_{cal}$ and these variables. For FeO, the R^2 value is ~0.2, presumably suggesting possible small errors caused by ignoring small amounts of Fe^{3+} in the high-P experimental products, as assumed in this study. For P_2O_5, the R^2 value is ~0.3, indicating a relatively poor performance of our high-P Ol geothermometer, which must be rooted in the limited P_2O_5 range of the high-P experimental melts (maximally ~0.38 wt%). This is however unimportant, since the P_2O_5 contents in common basaltic melts are usually low. In comparison, our room-P Ol geothermometer has a relatively weak performance in the case of Na_2O only, as indicated by the R^2 value of ~0.2. This must be due to the limited Na_2O range of the room-P experimental melts (maximally ~4.49 wt%), and should be solved by resorting to future experimental data with higher Na_2O contents in the basaltic melts.

Using the same experimental data as above, the performance of our Ol geothermometers has been compared with other geothermometers, and the result is summarized in Table 4. The selected geothermometers included Ford et al. (1983; Mg partition-based Ol geothermometer), Beattie (1993; Mg partition-based Ol geothermometer); Gudfinnsson and Presnall (2001; Mg partition-based Ol geothermometer, their Eq. (7)) and Lee et al. (2009; their Eq. (3) based on the reaction $Mg_2SiO_4^{Ol} + SiO_2^{liq} = Mg_2Si_2O_6^{Opx}$ where Opx stands for orthopyroxene in equilibrium with Ol and melt), in addition to Putirka et al. (2007; P2007-(2) and P2007-(4)). As suggested by Table 4, our Ol

Table 2
Range of melt compositions for calculating data.

n	Room P 69			High P 140		
	max	*min*	*avge*	*max*	*min*	*avge*
SiO_2	72.91	39.08	52.97	72.91	39.08	52.88
Al_2O_3	18.70	7.48	13.38	21.74	5.72	14.44
MgO	20.47	1.53	9.03	34.87	1.29	10.09
CaO	18.27	3.02	10.99	18.27	0.00	9.41
K_2O	10.64	0.04	1.94	14.83	0.04	2.95
FeO	14.86	0.00	6.23	14.86	0.00	6.08
Fe_2O_3	4.57	0.00	1.49	4.57	0.00	0.73
Na_2O	4.22	0.00	1.70	5.83	0.00	1.53
TiO_2	9.15	0.00	2.12	9.15	0.00	1.36
MnO	0.27	0.00	0.11	0.27	0.00	0.10
P_2O_5	0.70	0.00	0.15	1.19	0.00	0.12
Cr_2O_3	0.26	0.00	0.03	1.48	0.00	0.13
NiO	0.06	0.00	0.00	0.06	0.00	0.00
Total			100.14			99.82
T (°C)	1400	1087	1238	1950	1087	1230
P (GPa)	0.0001	0.0001	0.0001	7.00	0.0001	0.86

n, number of samples; *max*, maximum value; *min*, minimum value; *avge*, average value. All oxides are calculated as weight percent.

Table 3
Coefficients of the derived geothermometers for room pressure and high pressure.

	Room pressure		High pressure		Function
	Value	*s.e.*	Value	*s.e.*	
C_0	−2.4088	0.1793	−2.2769	0.2884	Constant
C_1	4662.9730	453.1027	3747.7671	678.6123	$1/T$
C_2	0.0000	0.0000	142.4796	25.7027	P/T
C_3	−1.0988	0.0435	−0.9002	0.0471	$\ln 1.5(Mg + Fe^{2+} + Ca + Mn + Ni)$
C_4	−0.4427	0.1604	0.5914	0.2655	$\ln 3Si$
C_5	−0.1706	0.4844	−0.7724	0.6286	$\ln(1 - Na)$
C_6	−1.0197	0.3847	0.9322	0.5441	$\ln(1 - K)$
C_7	0.4281	0.2702	−0.4970	0.4178	$\ln(1 - Al)$
C_8	1.4378	0.7922	−0.7551	1.6810	$\ln(1 - Fe^{3+})$
C_9	−1.5320	0.3257	−1.8204	0.4495	$\ln(1 - Ca)$
C_{10}	4.5867	3.7201	−12.8583	5.3171	$\ln(1 - P)$
C_{11}	−0.0352	0.9009	−4.0000	1.6456	$\ln(1 - Ti)$
C_{12}	−12.3614	10.8796	2.7330	5.4989	$\ln(1 - Cr^{3+})$
n	69		140		
s.d.	0.0292		0.0833		
r	0.9988		0.9933		

s.e., standard error; *n*, numbers of samples; *s.d.*, standard deviation in $lnD^{Ol/liq}_{MgO*}$; *r*, correlation coefficient; *T*, temperature (K); *P*, pressure (GPa). All elements are calculated in molar fractions.

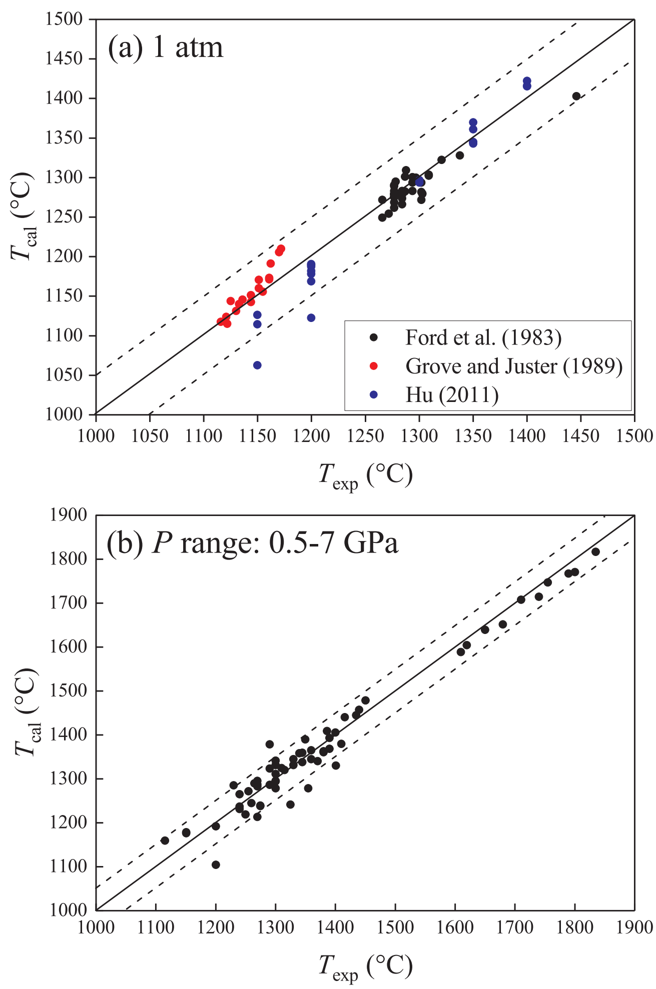

Fig. 3. Temperatures calculated (T_{cal}) by our new geothermometer compared to experimentally-measured values (T_{exp}): (a) 1 atm (75 data points); (b) high pressure (63 data points). Note that data from simple systems and complex rock compositions are lumped together in these plots.

geothermometers reproduced the T_{exp} with the highest accuracy: the R^2 value being close to 1, the slope between the T_{cal} and T_{exp} close to 1, and the average difference between the T_{cal} and T_{exp} the smallest, whatever the *P* is. Other conclusions that can be drawn from Table 4 are: (1) the Ol geothermometer of Ford et al. (1983) is good for low-*P* K_2O-rich magmas, but not for high-*P* K_2O-rich magmas; (2) the Ol geothermometer of Beattie (1993) gives out generally reasonable *T* estimates at low *P*, and slightly better *T* estimates than Ford et al. (1983) at high *P* conditions; (3) the Ol geothermometer of Gudfinnsson and Presnall (2001) has a very poor performance, and should not be applied to K_2O-rich magmas; (4) the geothermometer of Lee et al. (2009) works better than that of Gudfinnsson and Presnall (2001), but still reproduces the T_{exp} poorly; (5) the Eq. (2) of Putirka et al. (2007) estimates the T_{exp} to similar accuracies as the geothermometer of Lee et al. (2009) does, but the Eq. (4) of Putirka et al. (2007) has a significantly better performance.

Furthermore, to evaluate our Ol geothermometers more carefully, some extra Ol-melt pairs obtained from Snyder and Carmichael (1992), Mysen (2007), and Wang and Gaetani (2008) are used. As STable 4 shows, our Ol geothermometers have excellent performance: all data points are distributed along the 1:1 line well within a deviation of ± 50 °C (see SFigure 1 in STable 4) and the average of the absolute differences between the T_{cal} and T_{exp} is only 18(10) °C. Satisfactorily, there is also no clear correlation between the $T_{exp} - T_{cal}$ and the K_2O contents of the melt phase (see SFigure 2 in STable 4).

In summary, the above evaluation indicates that our Ol geothermometers are of high accuracy in reproducing the T_{exp}. To the contrary, relatively large differences between the T_{exp} and T_{cal} using most previous geothermometers exist both at room *P* and at high *P* conditions. These differences are clearly correlated with the K_2O contents of the melts. Our new Ol geothermometers successfully solve this problem (Fig. 4a and d), reproduce the T_{exp} very well (Fig. 3 and Table 4), and should be used in estimating the *T* of the potassium-rich silicate magmas in equilibrium with Ol.

5. Melt composition geothermometer

Our Ol geothermometers obtained above require both the compositions of the melt and coexisting Ol as inputs. However, the coexistence

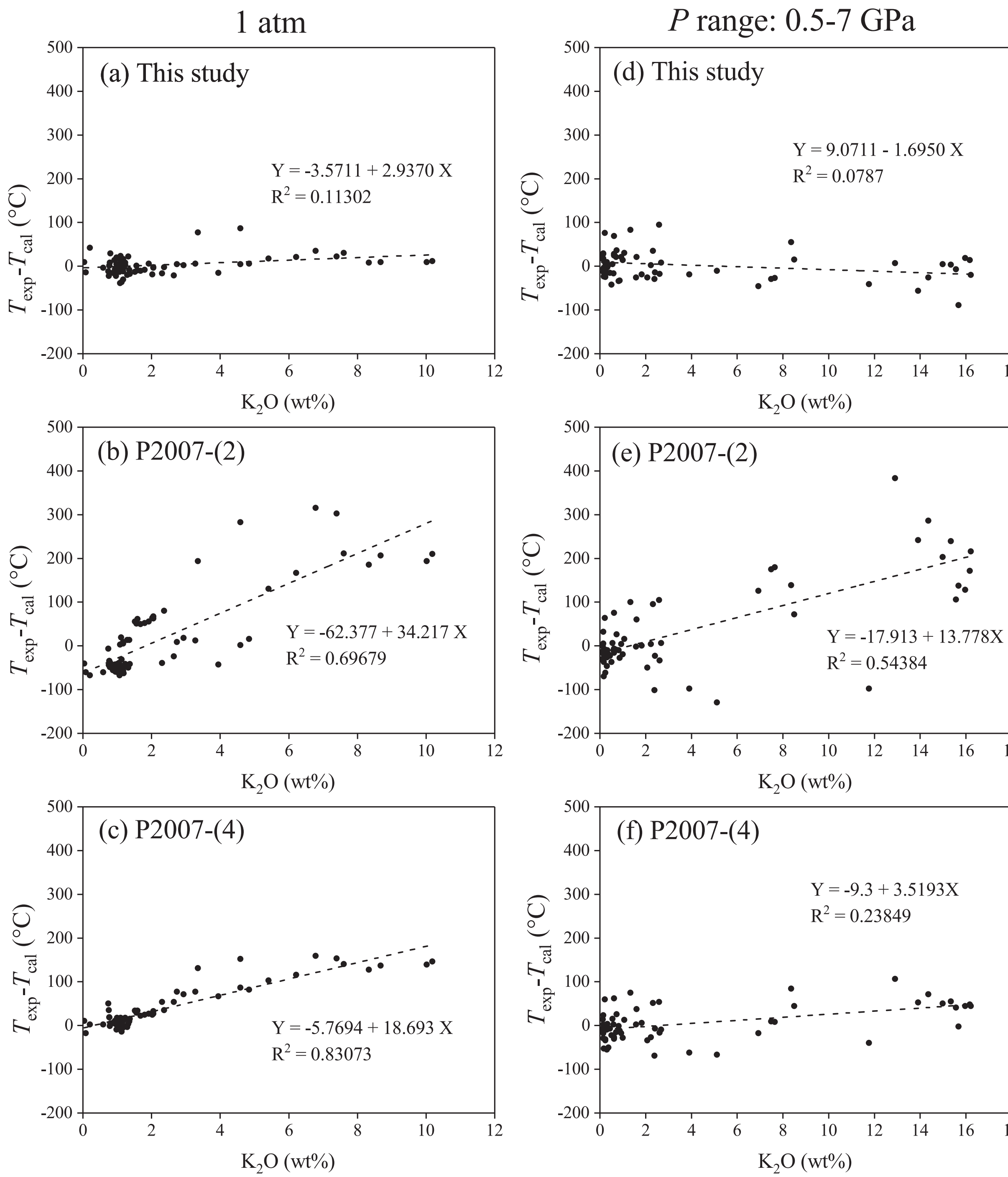

Fig. 4. K_2O contents vs temperature differences between T_{exp} and T_{cal} calculated by our geothermometer, P2007-(2) and P2007-(4): 1 atm (a, b, c) and high pressure (d, e, f). Sources of data (138 data) as in Fig. 3. P2007-(2) and P2007-(4) are Eq. (2) and Eq. (4) of Putirka et al. (2007), respectively.

of Ol with silicate magmas is not readily observed in some cases, and the composition of Ol is thus not always available. Roeder and Emslie (1970) demonstrated that the ratio of the partition coefficients for Fe^{2+} and Mg between Ol and melt at 1 atm was generally constant, $K_D = (X_{Fe}^{Ol}/X_{Fe}^{liq})/(X_{Mg}^{Ol}/X_{Mg}^{liq}) = \sim 0.30(3)$, implying the possibility of calculating the Ol composition from the melt composition alone (especially the FeO and MgO contents). In that case, one could derive a melt composition geothermometer with the melt composition as the only input. However, it was later found that the K_D was not only dependent on *T*, but also on *P* (Mysen, 1975; Ulmer, 1989) and melt composition (Longhi et al., 1978; Kushiro and Walter, 1998). Fig. 5 shows the K_D values of the Ol-melt pairs from the Group 2 (room *P*) and Group 3 (high *P*) of our database, varying from 0.24 to 0.51. This observation nullifies the feasibility of calculating the Ol composition from the melt composition by using a single and constant K_D, in good agreement with the finding of Gudfinnsson and Presnall (2001).

On the basis of combining the constraints of mineral stoichiometry with the relationships between partition coefficients, Beattie et al.

Table 4
Statistical analysis of calculated temperatures versus experimental temperatures.

Geothermometer	F1983	B1993	G2001	P2007-(2)	P2007-(4)	L2009	This study
Room *P*							
R^2	0.8795	0.8176	0.6948	0.7640	0.7882	0.7732	0.9381
Slope	0.7766	1.0035	2.3737	1.7299	1.1355	1.7151	1.0017
Intercept	295.65	−23.619	−1790.8	−928.73	−206.13	−876.10	−5.2386
Average	22	26	122	69	38	74	14
s.d.	25	33	133	68	47	59	15
High *P*							
R^2	0.2034	0.9344	0.6600	0.8240	0.9633	0.8155	0.9617
Slope	0.6921	1.2112	1.5471	1.2211	1.0946	1.1686	0.9540
Intercept	590.54	−231.26	−881.23	−340.58	−134.67	−284.97	60.925
Average	174	68	156	72	31	77	25
s.d.	232	54	189	81	24	80	21

Slope and Intercept, *a* and *b* of linear regression ($T_{exp} = a * T_{cal} + b$), respectively; Average and stand deviation (*s.d.*) are calculated using the absolute values of the differences between T_{cal} and T_{exp}. F1983, Ford et al. (1983); B1993, Beattie (1993); G2001, Gudfinnsson and Presnall (2001); P2007-(2), Eq. (2) in Putirka et al. (2007); P2007-(4), Eq. (4) in Putirka et al. (2007); L2009, Lee et al. (2009).

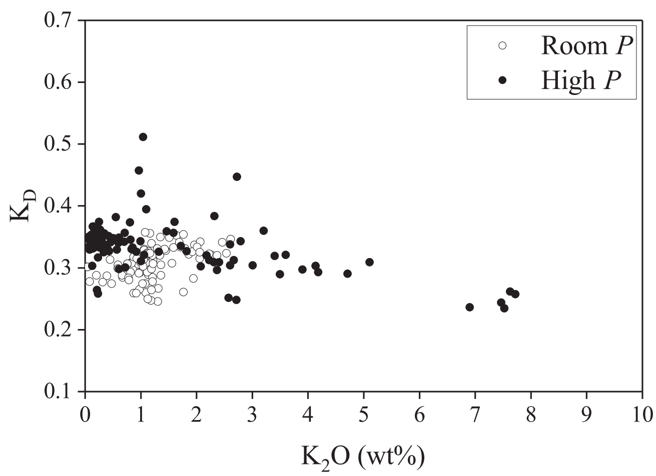

Fig. 5. K_2O (wt%) vs K_D values of the Ol-melt pairs from the Group 2 (room *P*; empty circles) and Group 3 (high *P*; filled circles) of our database.

(1991) developed another scheme for calculating the Ol composition from the melt composition. According to Beattie et al. (1991), the value of $D_{Mg}^{Ol/liq}$can be calculated using the following equation

$$D_{Mg}^{Ol/liq} = \frac{0.666{-}0.027X_{Fe^{2+}}^{liq} + 0.049X_{Mn}^{liq} + 0.385X_{Co}^{liq} + 3.665X_{Ni}^{liq}}{X_{Mg}^{liq} + 0.299X_{Fe^{2+}}^{liq} + 0.259X_{Mn}^{liq} + 0.786X_{Co}^{liq} + 3.346X_{Ni}^{liq}}, \quad (6)$$

where X_i^{liq} is the molar fraction of component *i* in the melt phase. The accuracy of this scheme, as claimed by Beattie et al. (1991), was better than ± 5% relative for the Mg partitioning between Ol and a silicate melt. We have followed the method of Beattie et al. (1991) in this study. By combining Eqs. (5) and (6), we have eventually derived a melt composition geothermometer which can be used to calculate the *T* by using the composition of the melt phase alone.

We have tested this melt composition geothermometer. The experimental data from Kushiro (1996), Liu and O'Neill (2004b) and Laporte et al. (2014) cover the *P* range from 0.5 to 3 GPa and *T* range from 1150 to 1500 °C ($n = 60$). Examination with these data (Fig. 6a) suggests that our melt composition geothermometer reproduces the T_{exp} very well: with the only few exceptions from Liu and O'Neill (2004b), all other data points fall in a deviation range of ± 50 °C. The relatively poor performance of the melt composition geothermometer on some of the experimental results of Liu and O'Neill (2004b) presumably reflects the fact that the present model could not properly process the Cr partition between the Ol and melt. In addition, there is a vague correlation between the $T_{exp} - T_{cal}$ and T_{exp} (Fig. 6a; higher T_{exp} accompanying higher *P* in general), as defined by the data of Kushiro

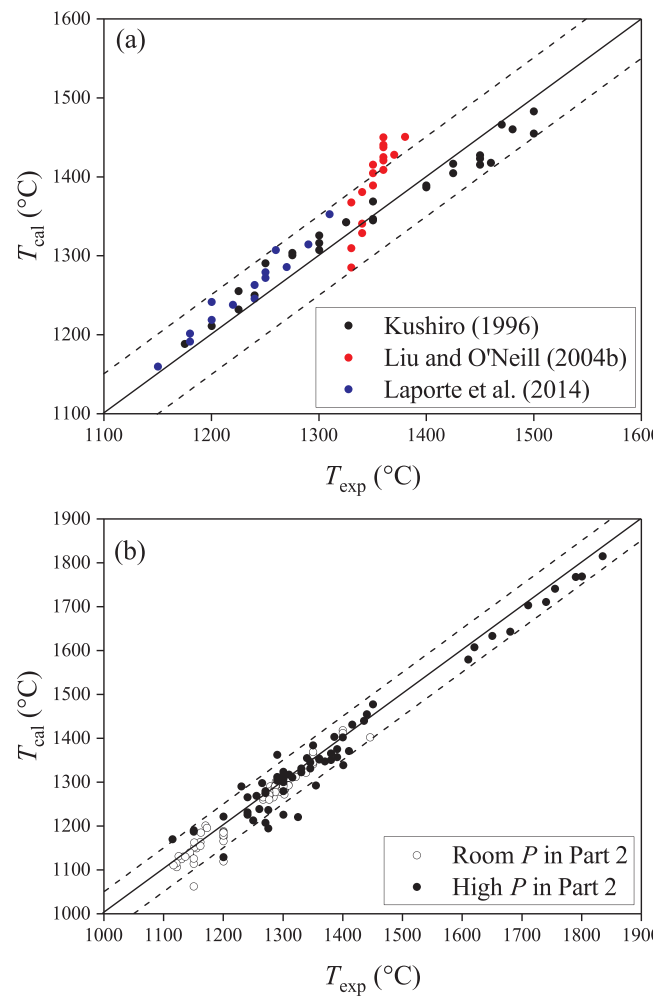

Fig. 6. Temperatures calculated (T_{cal}) by our melt composition geothermometer compared to measured values (T_{exp}). (a) Data from partial melting experiments of Kushiro (1996), Liu and O'Neill (2004b) and Laporte et al. (2014), covering the pressure range of 0.5–3 GPa; (b) Other data from Part 2 of our database conducted at room *P* (empty circles) and high *P* (filled circles), respectively.

(1996) and Laporte et al. (2014). Both studies aimed at the compositions of the melts at very low partial melting extents of peridotite, which might have been subject to some complexes in the equilibrium status. Furthermore, small amounts of water in the melt phase have little influence on the T_{cal}; the melt phase in Laporte et al. (2014) contained 0.02–1.15 wt% water.

We have further tested our melt composition geothermometer with all other data from Part 2 of our database (n = 138). The examination suggests that less than ~10 data points fall out of a deviation range of ± 50 °C, indicating an excellent performance of the melt composition geothermometer (Fig. 6b). The experiments showing relatively large differences between the T_{cal} and T_{exp} were usually conducted at low T_{exp}, so that their constitutional phases might have not achieved close chemical equilibrium. The melt phase in Laporte et al. (2004) also contained small amounts of water (0.28–1.13 wt%); a well reproduction of the T_{exp} by our melt composition geothermometer suggests, again, a negligible role of small amounts of water in the T estimation.

In summary, these tests verify our melt composition geothermometer, which allows the T estimate of silicate magma coexisting with Ol by using the composition of the melt alone.

6. Application: temperature of the Somma-Vesuvius magmas

The Somma-Vesuvius volcanic complex (SVVC), a Quaternary composite stratovolcano, locates ~15 km southeast of Naples, Italy. It became active ~0.3–0.5 million years ago (Santacroce et al., 2008), and was characterized by plinian and subplinian explosive eruptions interrupted by periods of closed conduit rest lasting up to ~1000 years (Cioni et al., 2003). For the last 22 ka, there have been four plinian caldera-forming eruptions (22 ka B.P. Pomici di Base, 8900 B.P. Mercato, 4300 B.P. Avellino, and A.D. 79 Pompeii; Santacroce et al., 2008) and at least three large subplinian eruptions (17.6 ka B.P. Pomici Verdoline, A.D. 472 Pollena, and A.D. 1631; Gurioli et al., 2010). The volcanic products of these major explosive eruptions younger than ~22 ka are mostly high potassium pyroclastics with widely variable SiO_2 contents (Fig. 7a), which can be divided into three series according to their age and composition: Series 1 being slightly SiO_2-undersaturated (normative nepheline < 5%) and older than 8900 B.P., Series 2 mildly SiO_2-undersaturated and from 8900 B.P. to A.D. 79, and Series 3 strongly SiO_2-undersaturated (leucite-normative) and younger than A.D. 79 (Joron et al., 1987; Ayuso et al., 1998; Santacroce et al., 2008). Evident among these high potassium pyroclastics (Fig. 7a), there was a drastic compositional change from early K-trachyte and K-phonolite (Series 1) to late leucititic phonolite (Series 3), primarily reflecting a difference in the replenishing magmas to the shallow magma chambers (a change from K-basaltic to K-tephritic magma; Santacroce et al., 2008). Additionally, Fig. 7a indicates a positive correlation between the K_2O-SiO_2 of the Series 1 magmas, demonstrating relatively complete evolutionary trends for the K-basaltic liquids initially driven by crystallization of mafic phases and plagioclase, and later controlled by fractionation of K-feldspar (Santacroce et al., 2008). To the contrary, the K_2O and SiO_2 contents of the Series 3 magmas show no apparent relationship, suggesting that the evolutionary trends of the K-tephritic liquids, frequently interrupted by new magma arrivals from deeper magma chambers, were dominated by crystallization of leucite and mafic minerals like clinopyroxene, amphibole and garnet, and characterized by minor role of plagioclase and the absence of K-feldspar fractionation. It follows that the magmas containing less K_2O and less SiO_2 should be more primitive, and record higher T.

As an exercise, we have applied our melt composition geothermometer to these high potassium pyroclastics. In the calculation, we assume a P value of 1 atm since the depths of the shallow magma chambers below the SVVC are commonly constrained as < 6 km (Cioni et al., 1998, 1999), with 1–2 km depths suggested for small magma chambers (Santacroce et al., 1993; Marianelli et al., 1995). This assumption should have little influence on our T estimation. Another factor potentially affecting the T estimation is the role of the water in the magmas. The water contents of the melt inclusions in the Ol and diopside phenocrysts from the high potassium pyroclastics are usually less than 2 wt%, occasionally reach ~3 wt% (Marianelli et al., 1995, 1999). Although our geothermometer does not have a specific term for water, our verification shown before has demonstrated its capability in accurately reproducing the T of the experiments which generated silicate melts with water contents up to ~1 wt% (Laporte et al., 2004, 2014). We speculate that the reason behind this phenomenon is probably due to the persistency of small amounts of water in the melts generated in nominally anhydrous high-P experiments (Liu et al., 2006), so that the effect of small amounts of water has been implicitly embedded in the geothermometer. Similar argument may apply to the role of possible CO_2 in the T estimation: because most high-P experiments with natural rock compositions have been conducted with the graphite or graphite + Pt capsules, a geothermometer calibrated with the compositional data of thus-produced melts may congenitally attain the capability handling the effects of small amounts of CO_2; anyhow, the CO_2 contents of the melt inclusions in the Ol phenocrysts have been constrained as usually < ~0.3 wt% (Marianelli et al., 1999). Another factor which needs critical evaluation is the coexistence of Ol with the high potassium pyroclastics. As summarized by Santacroce et al. (2008), the SVVC usually contains: (1) loose crystals of leucite and clinopyroxene, with garnet, biotite, amphibole, plagioclase and sanidine much less common; (2) leucite-bearing lava, with some intrusive and skarn rocks, and rare carbonate rocks; and (3) light/dark/greenish gray or brown/dark brown scoria or pumice. Evidently, the occurrence of the Ol phenocrysts is not ubiquitous. Additionally, the studies on the melt inclusions in the Ol and diopside phenocrysts suggest that the

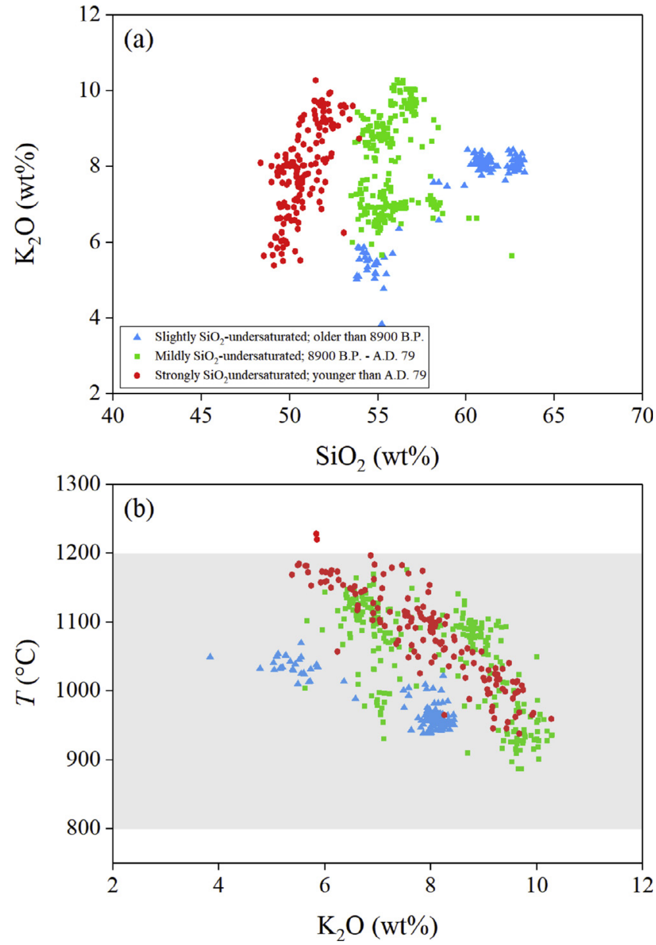

Fig. 7. High potassium igneous rocks from Somma-Vesuvius with ages younger than ~22 ka: (a) K_2O vs SiO_2 (wt%); (b) K_2O vs eruption temperatures calculated by our melt composition geothermometer. See Santacroce et al. (2008; references therein) for the plotted data. The shaded area represents the T range recorded by the melt inclusions in the clinopyroxene phenocrysts (Cioni et al., 1999).

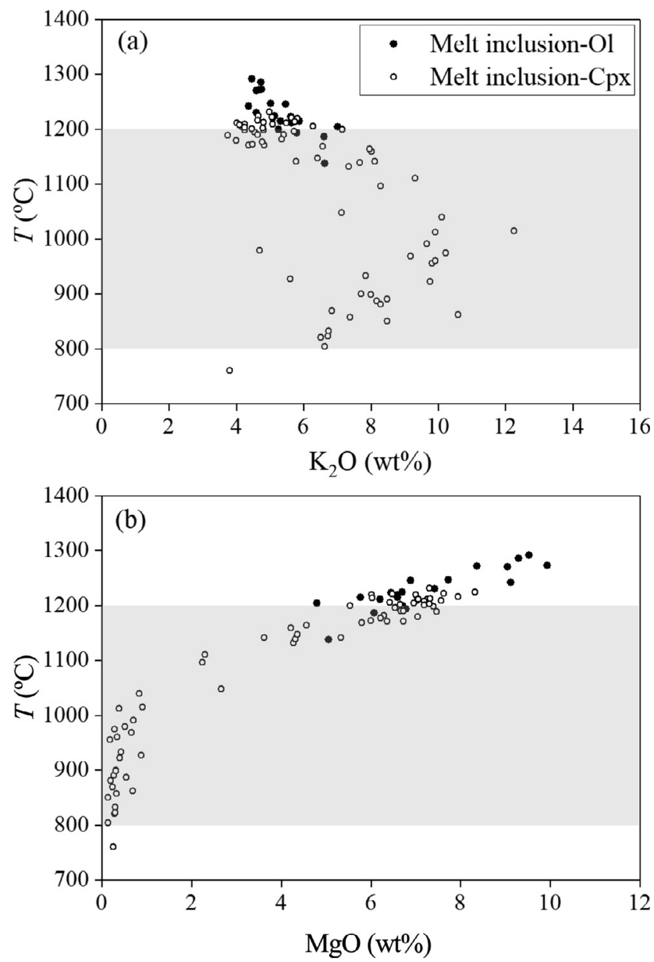

Fig. 8. Temperatures calculated by our melt composition geothermometer vs (a) K_2O (wt%); (b) MgO (wt%) for the melt inclusions in Ol and clinopyroxene (Cpx; mostly diopside) phenocrysts. The compositional data for the melt inclusions in the Ol are from Marianelli et al. (1995, 1999), and those for the melt inclusions in the Cpx are from Marianelli et al. (1995, 1999) and Cioni et al. (1998). The shaded areas in both (a) and (b) represent the T range recorded by the melt inclusions in the clinopyroxene phenocrysts (Cioni et al., 1999).

major Ol crystallization may dominantly take place at high T, with a MgO content > ~8 wt% in the silicate melts (Marianelli et al., 1995). Consequently, our melt composition geothermometer may be strictly applicable to the high-MgO melts only.

The result of the T estimation of these high potassium pyroclastics, in general agreement with the T records documented by the melt inclusions in clinopyroxene phenocrysts (800–1200 °C; Cioni et al., 1999), is shown in Fig. 7b: The T of the Series 1, Series 2, and Series 3 magmas ranges from 939 to 1070 °C (979(35)), from 887 to 1176 °C (1053(71)), and from 938 to 1228 °C (1080(68)), respectively. Along with the compositional change from early K-trachyte and K-phonolite (Series 1) to late leucititic phonolite (Series 3) is therefore an overall T increase. Presumably the high potassium pyroclastics of the Series 1 were from large and well-developed magma chambers with obstructed conduits, so that relatively extensive fractional crystallization took place, more evolved magmas formed, and low T was thus attained (Santacroce et al., 2008). In contrast, the high potassium pyroclastics of the Series 3 were perhaps from small and continually-tapped magma chambers with open conduits, characterized with frequently-interrupted fractional crystallization processes due to fresh magma replenishments from deeper magma chambers (Marianelli et al., 1999). The least-evolved magmas in the Series 3, with the minimum K_2O and SiO_2 contents and best chance in equilibrium with Ol, therefore recorded high magma T up to ~1228 °C (Fig. 7b), a T even higher than the T constrained by most melt inclusions in the diopside phenocrysts (800–1200 °C; Cioni et al., 1999).

Similarly, we have also applied our melt composition geothermometer to those melt inclusions in the Ol and diopside phenocrysts (Fig. 8). The homogenization T of the melt inclusions in the diopside phenocrysts ranged from 800 to 1200 °C (Cioni et al., 1998, 1999), in general agreement with our T estimates (760–1231 °C with an average of 1082 °C; 70 data points). The homogenization T of the melt inclusions in the Ol phenocrysts is largely unavailable, but should be higher than that of the melt inclusions in the diopside phenocrysts (Marianelli et al., 1995). Indeed, our T estimates for the melt inclusions in the Ol phenocrysts are higher, and vary from 1138 to 1292 °C (averagely 1230 °C; 20 data points). Furthermore, the correlation between the T estimates and the MgO contents strongly argues that the melt inclusions in the diopside phenocrysts span a large range of magma compositions (from slightly evolved to extensively crystallization-fractionized) whereas those in the Ol phenocrysts are much more primitive, especially those with MgO contents > 8 wt% (Fig. 8b). Additionally, the relationship between the T estimates and K_2O content of the melt inclusions in the diopside phenocrysts is complicated (Fig. 8a), implying that the K_2O content is not a good indicator for the magma evolution process of the SVVC, and its application should be avoided (Marianelli et al., 1999; Santacroce et al., 2008).

7. Conclusions

In this paper, we assembled a large number of experimental compositional data for the Ol-melt equilibrium pairs covering a large range of K_2O contents in the melts, a T range of 1087–1950 °C, and a P range of 0.0001–7.0 GPa, with some collected from the literature and some reported here for the first time. On the basis of the MgO partition between the Ol and K_2O-rich silicate melt, we successfully derived two K_2O-dependent Ol geothermometers applicable to high potassium magmas, one for 1 atm and one for the P range of 0.0001–7 GPa. We also derived one melt composition geothermometer which allows one to make T estimate by using the melt composition alone, provided that the melt is in equilibrium with the Ol phase at a known P.

Our examinations have shown that our geothermometers have excellent performance, with an average of 14 °C at room P and 25 °C at high P for the absolute differences between the T_{cal} and T_{exp}. The differences between the T_{cal} and T_{exp} show no clear dependence on the contents of K_2O (Fig. 4a and d) and any other oxides in the melts, P, and T. We recommend the application of our geothermometers in the T estimation of the Ol-bearing melts, especially for the high potassium silicate magmas.

The application of our melt composition geothermometer to the Somma-Vesuvius volcanic complex suggests that the geothermometers derived in this study can achieve reasonable T estimates for the high potassium silicate magmas, as along as the equilibrium between the Ol and melt is maintained. Small amounts of volatiles such as H_2O and CO_2 in the melts do not impair the good performance of our geothermometer.

Acknowledgements

We thank two anonymous reviewers for their insightful comments on our manuscript, and Prof. Jinhui Yang for his editorial handling of our paper. This study was financially supported by the Strategic Priority Research Program (B) of Chinese Academy of Sciences (Grant No. XDB18000000), by the DREAM project of MOST, China (Grant No. 2016YFC0600408), and by the Program of the Data Integration and Standardization in the Geological Science and Technology from MOST, China (Grant No. 2013FY1109000-3).

References

Ádám, A., 1978. Geothermal effects in the formation of electrically conducting zones and temperature distribution in the earth. Phys. Earth Planet. Int. 17, 21–28.
Anderson, O.L., 1980. The temperature profile of the upper mantle. J. Geophys. Res. [Atmos.] 85, 7003–7010.
Ayuso, R.A., De Vivo, B., Rolandi, G., Seal II, R.R., Paone, A., 1998. Geochemical and isotopic (Nd-Pd-Sr-O) variations bearing on the genesis of volcanic rocks from Vesuvius, Italy. J. Volcanol. Geotherm. Res. 82, 53–78.
Basu, A.R., Wang, J.W., Huang, W.K., Xie, G.H., Tatsumoto, M., 1991. Major element, REE, and Pb, Nd and Sr isotopic geochemistry of Cenozoic volcanic-rocks of eastern China-implications for their origin from suboceanic-type mantle reservoirs. Earth Planet. Sci. Lett. 105, 149–169.
Beattie, P., 1993. Olivine-melt and orthopyroxene-melt equilibria. Contrib. Mineral. Petrol. 115, 103–111.
Beattie, P., Ford, C., Russell, D., 1991. Partition coefficients for olivine-melt and orthopyroxene-melt systems. Contrib. Mineral. Petrol. 109, 212–224.
Birle, J.D., Gibbs, G.V., Moore, P.B., Smith, J.V., 1968. Crystal structure of natural olivines. Am. Miner. 53, 807–824.
Boyd, F.R., 1973. A pyroxene geotherm. Geochim. Cosmochim. Acta 37, 2533–2538.
Chen, J.C., Hsu, C.N., Ho, K.S., 2003. Geochemistry of Cenozoic volcanic rocks and related ultramafic xenoliths from the Jilin and Heilongjiang provinces, northeast China. J. Asian Earth Sci. 21, 1069–1084.
Chen, L.H., Zeng, G., Jiang, S.Y., Hofmann, A.W., Xu, X.S., Pan, M.B., 2009. Sources of Anfengshan basalts: subducted lower crust in the Sulu UHP belt, China. Earth Planet. Sci. Lett. 286, 426–435.
Chen, S.S., Fan, Q.C., Zou, H.B., Zhao, Y.W., Shi, R.D., 2015. Geochemical and Sr-Nd isotopic constraints on the petrogenesis of late Cenozoic basalts from the Abaga area, inner Mongolia, eastern China. J. Volcanol. Geotherm. Res. 305, 30–44.
Chen, X.Y., Liu, J.Q., Guo, Z.F., Lu, F., Jiang, D.H., 2008. A study on the geochemical characteristics and origin of volcanic rocks in Wangtian'e volcano. Acta Petrol. Sin. 24, 2576–2584.
Chen, Y., Zhang, Y., Graham, D., Su, S., Deng, J., 2007. Geochemistry of Cenozoic basalts and mantle xenoliths in Northeast China. Lithos 96, 108–126.
Chung, S.L., 1999. Trace element and isotope characteristics of Cenozoic basalts around the Tanlu fault with implications for the eastern plate boundary between North and South China. J. Geol. 107, 301–312.
Chung, S.L., Cheng, H., Jahn, B., Suzanne, Y., O'Reilly, Zhu, B., 1997. Major and trace element, and Sr-Nd isotope constraints on the origin of Paleogene volcanism in South China prior to the South China Sea opening. Lithos 40, 203–220.
Chung, S.L., Jahn, B.M., Chen, S.J., Lee, T., Chen, C.H., 1995. Miocene basalts in northwestern Taiwan: evidence for EM-type mantle sources in the continental lithosphere. Geochim. Cosmochim. Acta 59, 549–555.
Chuvashova, I.S., Rasskazov, S.V., Yasnygina, T.A., Saranina, E.V., Fefelov, N.N., 2007. Holocene volcanism in central Mongolia and northeast China: asynchronous decompressional and fluid melting of the mantle. J. Volcanol. Seismol. 1, 372–396.
Chu, Z.Y., Harvey, J., Liu, C.Z., Guo, J.H., Wu, F.Y., Tian, W., 2013. Source of highly potassium basalts in northeast China: evidence from Re-Os, Sr-Nd-Hf isotopes and PGE geochemistry. Chem. Geol. 357, 52–66.
Cioni, R., Marianelli, P., Santacroce, R., 1998. Thermal and compositional evolution of the shallow magma chambers of Vesuvius: evidence from pyroxene phenocrysts and melt inclusions. J. Geophys. Res. 103, 18277–18294.
Cioni, R., Marianelli, P., Santacroce, R., 1999. Temperature of Vesuvius magmas. Geology 27, 443–446.
Cioni, R., Sulpizio, R., Garruccio, N., 2003. Variability of the eruption dynamics during a Subplinian event: the Greenish Pumice eruption of Somma-Vesuvius (Italy). J. Volcanol. Geotherm. Res. 124, 89–114.
Conceição, R.V., Green, D.H., 2000. Behavior of the cotectic curve En-Ol in the system leucite-olivine-quartz under dry conditions to 2.0 GPa. Geochem. Geophys. Geosyst. 1, 185–202.
Cong, B., Guo, J.H., Liu, W.J., 2001. A possible relict mantle wedge: geochemical evidence from paleogene volcanics in north China. Chin. Sci. Bull. 46, 1917–1922.
Cong, B.L., Wang, Q.C., Zhang, H.Z., Yan, X., Jiang, L.L., 1996. Petrogenesis of Cenozoic volcanic rocks in Hefei basin, China. Acta Petrol. Sin. 12, 370–381 (in Chinese).
Conticelli, S., Peccerillo, A., 1992. Petrology and geochemistry of potassium and ultrapotassium volcanism in central Italy: petrogenesis and inferences on the evolution of the mantle source. Lithos 28, 221–240.
Davis, F.A., Hirschmann, M.M., 2013. The effects of K_2O on the compositions of near-solidus melts of garnet peridotite at 3 GPa and the origin of basalts from enriched mantle. Contrib. Mineral. Petrol. 166, 1029–1046.
Draper, D.S., Green, T.H., 1997. P-T phase relations of silicic, alkaline, aluminous mantle-xenolith glasses under anhydrous and C-O-H fluid-saturated conditions. J. Petrol. 38, 1187–1224.
Draper, D.S., Green, T.H., 1999. P-T, phase relations of silicic, alkaline, aluminous liquids: new results and applications to mantle melting and metasomatism. Earth Planet. Sci. Lett. 170, 255–268.
Draper, D.S., Johnston, A.D., 1992. Anhydrous PT phase relations of an Aleutian high-MgO basalt: an investigation of the role of olivine-liquid reaction in the generation of arc high-alumina basalts. Contrib. Mineral. Petrol. 112, 501–519.
Falloon, T.J., Danyushevsky, L.V., Ariskin, A., Green, D.H., Ford, C.E., 2007. The application of olivine geothermometry to infer crystallization temperatures of parental liquids: implications for the temperature of MORB magmas. Chem. Geol. 241, 207–233.
Fan, Q.C., Hooper, P.R., 1991. The Cenozoic basaltic rocks of eastern China: petrology and chemical composition. J. Petrol. 32, 765–810.
Fan, Q.C., Liu, R.X., Li, D.M., Li, Q., 1999. Significance of K-Ar age of bimodal volcanic rocks at Wangtian'e volcano, Changbaishan area. Chin. Sci. Bull. 44, 660–663.
Fan, Q.C., Liu, R.X., Zhang, G.H., Sui, J.L., 1998. The genesis and evolution of bimodal volcanic rocks in Wangtian'e volcano, Changbaishan. Acta Petrol. Sin. 14, 305–317 (in Chinese).
Fan, Q.C., Sui, J.L., Wang, T.H., Li, N., Sun, Q., 2006a. Eruption history and magma evolution of the trachybasalt in the Tianchi volcano, Changbaishan. Acta Petrol. Sin. 22, 1449–1457 (in Chinese).
Fan, Q.C., Sui, J.L., Wang, T.H., Li, N., Sun, Q., 2007. History of volcanic activity, magma evolution and eruptive mechanisms of the Changbai volcanic province. Geol. J. China Univ. 13, 175–190 (in Chinese).
Fan, Q.C., Sun, Q., Li, N., Wang, T.H., 2006b. Holocene volcanic rocks in Jingbo lake region diversity of magmatism. Prog. Nat. Sci. 16, 65–71.
Ford, C.E., Russell, D.G., Craven, J.A., Fisk, M.R., 1983. Olivine liquid equilibria: temperature, pressure and composition dependence of the crystal/liquid cation partition coefficients for Mg, Fe^{2+}, Ca and Mn. J. Petrol. 24, 256–265.
Fraser, D.G., 1977. Thermodynamic properties of silicate melts. In: Fraser, D.G. (Ed.), Thermodynamics in Geology. Reidel, Holland, pp. 301–325.
Green, D.H., Ringwood, A.E., 1967. The genesis of basaltic magmas. Contrib. Mineral. Petrol. 15, 103–190.
Grove, T.L., Juster, T.C., 1989. Experimental investigations of low-Ca pyroxene stability and olivine-pyroxene-liquid equilibria at 1-atm in natural basaltic and andesitic liquids. Contrib. Mineral. Petrol. 103, 287–305.
Gudfinnsson, G.H., Presnall, D.C., 2001. A pressure-independent geothermometer for primitive mantle melts. J. Geophys. Res. 106, 16205–16211.
Guo, H., Xia, B., Wang, R.H., Wang, Q., Wang, J.J., 2006. Geochemistry and geotectonic significance of Eogene basalts in Yangxin Area, Bohai Bay basin. Geochemistry 35, 221–226 (in Chinese).
Gurioli, L., Sulpizio, R., Cioni, R., Sbrana, A., Santacroce, R., Luperini, W., Andronico, D., 2010. Pyroclastic flow hazard assessment at Somma-Vesuvius based on the geological record. Bull. Volcanol. 72, 1021–1038.
Han, B.F., Wang, S.G., Kagami, H., 1999. Trace element and Nd-Sr isotope constraints on origin of the Chifeng flood basalts, north China. Chem. Geol. 155, 187–199.
Hart, S.R., Davis, K.E., 1978. Nickel partitioning between olivine and silicate melt. Earth Planet. Sci. Lett. 40, 203–219.
Herzberg, C., O'Hara, M.J., 2002. Plume-associated ultramafic magmas of Phanerozoic Age. J. Petrol. 43, 1857–1883.
Herzberg, C.T., 1979. The solubility of olivine in basaltic liquids: an ionic model. Geochim. Cosmochim. Acta 43, 1241–1251.
Hirschmann, M.M., Baker, M.B., Stolper, E.M., 1998. The effect of alkalis on the silica content of mantle-derived melts. Geochim. Cosmochim. Acta 62, 883–902.
Ho, K.S., Chen, J.C., Juang, W.S., 2000. Geochronology and geochemistry of late Cenozoic basalts from the Leiqiong area, southern China. J. Asian Earth Sci. 18, 307–324.
Ho, K.S., Chen, J.C., Lo, C.H., Zhao, H.L., 2003. ^{40}Ar-^{39}Ar dating and geochemical characteristics of late Cenozoic basaltic rocks from the Zhejiang-Fujian region, SE China: eruption ages, magma evolution and petrogenesis. Chem. Geol. 197, 287–318.
Ho, K.S., Ge, W.C., Chen, J.C., You, C.F., Yang, H.J., Zhang, Y.L., 2013. Late Cenozoic magmatic transitions in the central great Xing'an range, northeast China: geochemical and isotopic constraints on petrogenesis. Chem. Geol. 352, 1–18.
Ho, K.S., Liu, Y., Chen, J.C., Yang, H.J., 2008. Elemental and Sr-Nd-Pb isotopic compositions of late Cenozoic Abaga basalts, Inner Mongolia: implications for petrogenesis and mantle process. Geochem. J. 42, 339–357.
Ho, K.S., Liu, Y., Chen, J.C., You, C.F., Yang, H.J., 2011. Geochemical characteristics of Cenozoic Jining basalts of the western north China craton: evidence for the role of the lower crust, lithosphere, and asthenosphere in petrogenesis. Terr. Atmos. Ocean. Sci. 22, 15–40.
Hong, L.B., Zhang, Y.H., Qian, S.P., Liu, J.Q., Ren, Z.Y., Xu, Y.G., 2013. Constraints from melt inclusions and their host olivines on the petrogenesis of Oligocene-early Miocene Xindian basalts, Chifeng area, north China craton. Contrib. Mineral. Petrol. 165, 305–326.
Hsu, C.N., Chen, J.C., 1998. Geochemistry of late Cenozoic basalts from Wudalianchi and Jingpohu areas, Heilongjiang Province, northeast China. J. Asian Earth Sci. 16, 385–405.
Hsu, C.N., Chen, J.C., Ho, K.S., 2000. Geochemistry of Cenozoic volcanic rocks from Kirin province, northeast China. Geochem. J. 34, 33–58.
Huang, J., Li, S.G., Xiao, Y.L., Ke, S., Li, W.Y., Tian, Y., 2015. Origin of low $\delta^{26}Mg$ Cenozoic basalts from south China block and their geodynamic implications. Geochim. Cosmochim. Acta 164, 298–317.
Hu, X.M., 2011. Partial melting of lherzolite in the system CaO-MgO-Al_2O_3-SiO_2-K_2O at 1 atm. Master thesis. Peking University.
Irvine, T.N., Kushiro, I., 1976. Partitioning of Ni and Mg between olivine and silicate liquids. Carnegie Inst. Washington Yearb. 75, 668–675.
Jaques, A.L., Green, D.H., 1980. Anhydrous melting of peridotite at 0–15 kb pressure and the genesis of tholeiitic basalts. Contrib. Mineral. Petrol. 73, 287–310.
Joron, J.L., Metrich, N., Rosi, M., Santacroce, R., Sbrana, A., 1987. Chemistry and petrography. In: Santacroce, R. (Ed.), Somma-Vesuvius. Quaderni de la ricerca scientifica, vol. 114, pp. 105–174.
Kinzler, R.J., 1997. Melting of mantle peridotite at pressures approaching the spinel to garnet transition: application to mid-ocean ridge basalt petrogenesis. J. Geophys. Res. 102, 853–874.
Kress, V.C., Carmichael, I.S.E., 1988. Stoichiometry of the iron oxidation reaction in silicate melts. Am. Miner. 73, 1267–1274.
Kuritani, T., Kimura, J.I., Miyamoto, T., Wei, H.Q., Shimano, T., Maeno, F., Jin, X., Taniguchi, H., 2009. Intraplate magmatism related to deceleration of upwelling asthenospheric mantle: implications from the Changbaishan shield basalts, northeast China. Lithos 112, 247–258.

Kuritani, T., Kimura, J.I., Ohtani, E., Miyamoto, H., Furuyama, K., 2013. Transition zone origin of potassium basalts from Wudalianchi volcano, northeast China. Lithos 156–159, 1–12.

Kuritani, T., Ohtani, E., Kimura, J.I., 2011. Intensive hydration of the mantle transition zone beneath China caused by slab stagnation. Nature Geosci. 4, 713–716.

Kushiro, I., 1996. Partial melting of a fertile mantle peridotite at high pressures: an experimental study using aggregates of diamond. In: Basu, A., Hart, S. (Eds.), Earth Process: Reading the Isotopic Code. Geophys. Monogr. AGU, 95, pp. 109–122.

Kushiro, I., Walter, M.J., 1998. Mg-Fe partitioning between olivine and mafic-ultramafic melts. Geophys. Res. Lett. 25, 2337–2340.

Laporte, D., Lambart, S., Schiano, P., Ottolini, L., 2014. Experimental derivation of nepheline syenite and phonolite liquids by partial melting of upper mantle peridotites. Earth Planet. Sci. Lett. 404, 319–331.

Laporte, D., Toplis, M.J., Seyler, M., Devidal, J.L., 2004. A new experimental technique for extracting liquids from peridotite at very low degrees of melting: application to partial melting of depleted peridotite. Contrib. Mineral. Petrol. 146, 463–484.

Lee, C.T.A., Luffi, P., Plank, T., Dalton, H., Leeman, W.P., 2009. Constraints on the depths and temperatures of basaltic magma generation on Earth and other terrestrial planets using new thermobarometers for mafic magmas. Earth Planet. Sci. Lett. 279, 20–33.

Leeman, W.P., 1978. Distribution of Mg^{2+} between olivine and silicate melt, and its implications regarding melt structure. Geochim. Cosmochim. Acta 42, 789–800.

Lee, Y.T., Chen, J.C., Shih, J.Y., Ho, K.S., Yang, H.J., Lin, M.L., Hu, Y.T., Chiu, C.H., 2013. Petrogenesis of Cenozoic basaltic rocks from Jiangsu province, China: evidence from geochemical constraints. Acta Geol. Sin. 87, 102–117.

Lee, Y.T., Chen, J.C., Shih, J.Y., Juang, W.S., Yang, H.J., Huang, S.W., Lin, M.L., 2006. Geochemistry of Cenozoic basaltic rocks from Shandong province and its implication for mantle process in north China. Geochem. J. 40, 579–596.

Li, H.Y., Huang, X.L., Guo, H., 2014. Geochemistry of Cenozoic basalts from the Bohai bay basin: implications for a heterogeneous mantle source and lithospheric evolution beneath the eastern north China craton. Lithos 196–197, 54–66.

Li, H.Y., Xu, Y.G., Ryan, J.G., Huang, X.L., Ren, Z.Y., Guo, H., Ning, Z.G., 2016a. Olivine and melt inclusion chemical constraints on the source of intracontinental basalts from the eastern north China craton: discrimination of contributions from the subducted pacific slab. Geochim. Cosmochim. Acta 178, 1–19.

Li, H.Y., Xu, Y.G., Ryan, J.G., Whattam, S.A., 2017. Evolution of the mantle beneath the eastern north China craton during the Cenozoic: linking geochemical and geophysical observations. J. Geophys. Res. 122, 224–246.

Liu, C.Q., Masuda, A., Xie, G.H., 1994. Major- and trace-element compositions of Cenozoic basalts in eastern China: petrogenesis and mantle source. Chem. Geol. 114, 19–42.

Liu, C.Q., Xie, G.H., Masuda, A., Shimizu, H., Takahashi, K., 1992. Effect of pressure on the peak position in the REE partition pattern: evidence from megacryst minerals in Kuandian and Hannuoba basalts. Geochimica 1, 19–33 (in Chinese).

Liu, J.Q., Chen, L.H., Wang, X.J., Zhong, Y., Yu, X., Zeng, G., Erdmann, S., 2017. The role of melt-rock interaction in the formation of Quaternary high-MgO potassium basalt from the greater Khingan range, northeast China. J. Geophys. Res. 122, 224–246.

Liu, J.Q., Chen, S.S., Guo, Z.F., Guo, W.F., He, H.Y., You, H.T., Kim, H.M., Sung, G.H., Kim, H.N., 2015. Geological background and geodynamic mechanism of Mt. Changbai volcanoes on the China-Korea border. Lithos 236–237, 46–73.

Liu, X., O'Neill, H., St, C., 2004a. Partial melting of spinel lherzolite in the system CaO-MgO-Al_2O_3-SiO_2 $\pm$ K_2O at 1.1 GPa. J. Petrol. 45, 1339–1368.

Liu, X., O'Neill, H., St, C., 2004b. The effect of Cr_2O_3 on the partial melting of spinel lherzolite in the system CaO-MgO-Al_2O_3-SiO_2-Cr_2O_3 at 1.1 GPa. J. Petrol. 45, 2261–2286.

Liu, X., O'Neill, H., St, C., Berry, A.J., 2006. The effects of small amounts of H_2O, CO_2 and Na_2O on the partial melting of spinel lherzolite in the system CaO-MgO-Al_2O_3-SiO_2 $\pm$ H_2O $\pm$ CO_2 $\pm$ Na_2O at 1.1 GPa. J. Petrol. 47, 409–434.

Liu, Y.S., Gao, S., Kelemen, P.B., Xu, W.L., 2008. Recycled crust controls contrasting source compositions of Mesozoic and Cenozoic basalts in the north China craton. Geochim. Cosmochim. Acta 72, 2349–2376.

Li, Y.Q., Ma, C.Q., Robinson, P.T., 2016b. Petrology and geochemistry of Cenozoic intraplate basalts in east-central China: constraints on recycling of an oceanic slab in the source region. Lithos 262, 27–43.

Longhi, J., Walker, D., Hays, J.F., 1978. The distribution of Fe and Mg between olivine and lunar basaltic liquids. Geochim. Cosmochim. Acta 42, 1545–1558.

Luo, D., Chen, L.H., Zeng, G., 2009. Genesis of intra-continental strongly alkaline volcanic rocks: a case study of Dashan nephelinites in Wudi, Shandong province, north China, Acta Petrol. Sin. 25, 311–319 (in Chinese).

Luth, W.C., 1967. The system $KAlSiO_4$-Mg_2SiO_4-$KAlSi_2O_6$. J. Am. Ceram. Soc. 50, 174–176.

Marianelli, P., Métrich, N., Santacroce, R., Sbrana, A., 1995. Mafic magma batches at Vesuvius: a glass inclusion approach to the modalities of feeding stratovolcanoes. Contrib. Mineral. Petrol. 120, 159–169.

Marianelli, P., Métrich, N., Sbrana, A., 1999. Shallow and deep reservoirs involved in magma supply of the 1944 eruption of Vesuvius. Bull. Volcanol. 61, 48–63.

Médard, E., Mccammon, C.A., Barr, J.A., Grove, T.L., 2008. Oxygen fugacity, temperature reproducibility, and H_2O contents of nominally anhydrous piston-cylinder experiments using graphite capsules. Am. Miner. 93, 1838–1844.

Mysen, B., 1975. Partitioning of iron and magnesium between crystals and partial melts in peridotite upper mantle. Contrib. Mineral. Petrol. 52, 69–76.

Mysen, B., 2007. Partitioning of calcium, magnesium, and transition metals between olivine and melt governed by the structure of the silicate melt at ambient pressure. Am. Miner. 92, 844–862.

Nielsen, R.L., 1988. TRACE.FOR: a program for the calculation of combined major and trace-element liquid lines of descent for natural magmatic systems. Comp. Geosci. 14, 15–35.

O'Neill, H., St, C., Wood, B.J., 1979. An experimental study of Fe-Mg partitioning between garnet and olivine and its calibration as a geothermometer. Contrib. Mineral. Petrol. 70, 59–70.

Presnall, D.C., Dixon, S.A., Dixon, J.R., O'Donnell, T.H., Brenner, N.L., Schrock, R.L., Dycus, D.W., 1978. Liquidus phase relations on the join diopside-forsterite-anorthite from 1 atm to 20 kbar: their bearing on the generation and crystallization of basaltic magma. Contrib. Mineral. Petrol. 66, 203–220.

Putirka, K.D., 2005. Mantle potential temperatures at Hawaii, Iceland, and the mid-ocean ridge system, as inferred from olivine phenocrysts: evidence for thermally driven mantle plumes. Geochem. Geophys. Geosyst. 6, 241–254.

Putirka, K.D., Perfit, M., Ryerson, F.J., Jackson, M.G., 2007. Ambient and excess mantle temperatures, olivine thermometry, and active vs. passive upwelling. Chem. Geol. 241, 177–206.

Qi, Q., Taylor, L.A., Zhou, X.M., 1994. Geochemistry and petrogenesis of three series of Cenozoic basalts from southeastern China. Int. Geol. Rev. 36, 435–451.

Rasskazov, S.V., Chuvashova, I.S., Liu, Y., Meng, F., Yasnygina, T.A., Fefelov, N.N., Saranina, E.V., 2011. Proportions of lithospheric and asthenospheric components in late Cenozoic K and K-Na lavas in Heilongjiang province, northeastern China. Petrology 19, 568–600.

Roeder, P.L., 1974. Activity of iron and olivine solubility in basaltic liquids. Earth Planet. Sci. Lett. 23, 397–410.

Roeder, P.L., Emslie, R.F., 1970. Olivine-liquid equilibrium. Contrib. Mineral. Petrol. 19, 275–289.

Sack, R.O., Walker, D., Carmichael, I.S.E., 1987. Experimental petrology of alkalic lavas: constraints on cotectics of multiple saturation in natural basic liquids. Contrib. Mineral. Petrol. 96, 1–23.

Sakuyama, T., Tian, W., Kimura, J.I., Fukao, Y., Hirahara, Y., Takahashi, T., Senda, R., Chang, Q., Miyazaki, T., Masayuki, O., Kawabata, H., Tatsumi, Y., 2013. Melting of dehydrated oceanic crust from the stagnant slab and of the hydrated mantle transition zone: constraints from Cenozoic alkaline basalts in eastern China. Chem. Geol. 359, 32–48.

Santacroce, R., Bertagnini, A., Civetta, L., Landi, P., Sbrana, A., 1993. Eruptive dynamics and petrogenetic processes in a very shallow magma reservoir: the 1906 eruption of Vesuvius. J. Petrol. 34, 383–425.

Santacroce, R., Cioni, R., Marianelli, P., Sbrana, A., Sulpizio, R., Zanchetta, G., Donahue, D.J., Joron, J.L., 2008. Age and whole rock-glass compositions of proximal pyroclastics from the major explosive eruptions of Somma-Vesuvius: a review as a tool for distal tephrostratigraphy. J. Volcanol. Geotherm. Res. 177, 1–18.

Schairer, J.F., 1954. The system K_2O-MgO-Al_2O_3-SiO_2: I, results of quenching experiments on four joins in the tetrahedron cordierite-forsterite-leucite-silica and on the join cordierite-mullite-potash feldspar. J. Am. Ceram. Soc. 37, 501–533.

Schwab, B.E., Johnston, A.D., 2001. Melting systematics of modally variable, compositionally intermediate peridotites and the effects of mineral fertility. J. Petrol. 42, 1789–1811.

Shankland, T.J., Ander, M.E., 1983. Electrical conductivity, temperature and fluids in the crust. J. Geophys. Res. 88, 9475–9484.

Snyder, D.A., Carmichael, I.S.E., 1992. Olivine-liquid equilibria and the chemical activities of FeO, NiO, Fe_2O_3, and MgO in natural basic melts. Geochim. Cosmochim. Acta 56, 303–318.

Sugawara, T., 2000. Empirical relationships between temperature, pressure, and MgO content in olivine and pyroxene saturated liquid. J. Geophys. Res. 105, 8457–8472.

Sun, Y., Ying, J.F., Zhou, X.H., Shao, J.A., Chu, Z.Y., Su, B.X., 2014. Geochemistry of ultrapotassium volcanic rocks in Xiaogulihe NE China: implications for the role of ancient subducted sediments. Lithos 208–209, 53–66.

Tang, Y.J., Zhang, H.F., Ying, J.F., 2006. Asthenosphere-lithospheric mantle interaction in an extensional regime: implication from the geochemistry of Cenozoic basalts from Taihang Mountains, North China Craton. Chem. Geol. 233, 309–327.

Ulmer, P., 1989. The dependence of the Fe^{2+}-Mg cation partitioning between olivine and basaltic liquid on pressure, temperature and composition. Contrib. Mineral. Petrol. 101, 261–273.

Walter, M.J., 1998. Melting of garnet peridotite and the origin of komatiite and depleted lithosphere. J. Petrol. 39, 29–60.

Walter, M.J., Presnall, D.C., 1994. Melting behaviour of simplified lherzolite in the system CaO-MgO-Al_2O_3-SiO_2-Na_2O from 7 to 35 kbar. J. Petrol. 35, 329–359.

Wang, X.J., Chen, L.H., Hofmann, A.W., Mao, F.G., Liu, J.Q., Zhong, Y., Xie, L.W., Yang, Y.H., 2017. Mantle transition zone-derived em1 component beneath NE China: geochemical evidence from Cenozoic potassium basalts. Earth Planet. Sci. Lett. 465, 16–28.

Wang, Y., Zhao, Z.F., Zheng, Y.F., Zhang, J.J., 2011. Geochemical constraints on the nature of mantle source for Cenozoic continental basalts in east-central China. Lithos 125, 940–955.

Wang, Z.R., Gaetani, G.A., 2008. Partitioning of Ni between olivine and siliceous eclogite partial melt: experimental constraints on the mantle source of Hawaiian basalts. Contrib. Mineral. Petrol. 156, 661–678.

Wasylenki, L.E., Baker, M.B., Kent, A.J.R., Stolper, E.M., 2003. Near-solidus melting of the shallow upper mantle: partial melting experiments on depleted peridotite. J. Petrol. 44, 1163–1191.

Watson, E.B., 1977. Partitioning of manganese between fosterite and silicate liquid. Geochim. Cosmochim. Acta 41, 1363–1374.

Wiser, N.M., Wood, B.J., 1991. Experimental determination of activities in Fe-Mg olivine at 1400 K. Contrib. Mineral. Petrol. 108, 146–153.

Wu, C.Z., Gu, L.X., Ren, Z.W., Zhang, Z.Z., Chen, Z.Y., Ming, Z., 2005. Transition from plate margin to intraplate environment: geochemistry of basalts in Paleogene Liaohe basin, northeastern China. Sci. China Ser. D Earth Sci. 48, 2069–2080.

Xu, Y.G., Chung, S.L., Ma, J.L., Shi, L.B., 2004. Contrasting Cenozoic lithospheric evolution and architecture in the western and eastern Sino-Korean craton: constraints

from geochemistry of basalts and mantle xenoliths. J. Geol. 112, 593–605.
Xu, Y.G., Ma, J.L., Frey, F.A., Feigenson, M.D., Liu, J.F., 2005. Role of lithosphere-asthenosphere interaction in the genesis of Quaternary alkali and tholeiitic basalts from Datong, western North China Craton. Chem. Geol. 224, 247–271.
Xu, Y.G., Zhang, H.H., Qiu, H.N., Ge, W.C., Wu, F.Y., 2012a. Oceanic crust components in continental basalts from Shuangliao, Northeast China: derived from the mantle transition zone? Chem. Geol. 328, 168–184.
Xu, Z., Zhao, Z.F., Zheng, Y.F., 2012b. Slab-mantle interaction for thinning of cratonic lithospheric mantle in north China: geochemical evidence from Cenozoic continental basalts in central Shandong. Lithos 146–147, 202–217.
Yang, Z.L., Tao, K.Y., Shen, W.Z., Wang, L.B., Yang, X.Z., 1998. Geochemistry and source characters of the concealed Eogene basalts in north Jiangsu basin. Acta Petrol. Sin. 14, 332–342 (in Chinese).
Yan, J., Zhao, J.X., 2008. Cenozoic alkali basalts from Jingpohu, NE China: the role of lithosphere-asthenosphere interaction. J. Asian Earth Sci. 33, 106–121.
Yan, J., Zhao, J.X., Liu, H.Q., 2007. Quaternary basalts from Longgang in the north China craton: petrologenesis and characteristics of the mantle source. Acta Petrol. Sin. 23, 1413–1422 (in Chinese).
Yu, X., Chen, L.H., Zeng, G., 2015a. Growing magma chambers control the distribution of small-scale flood basalts. Sci. Rep. 5. https://doi.org/10.1038/srep16824.
Yu, X., Lee, C.A., Chen, L.H., Zeng, G., 2015b. Magmatic recharge in continental flood basalts: insights from the Chifeng igneous province in inner Mongolia. Geochem. Geophys. Geosyst. 16, 2082–2096.
Zeng, G., Chen, L.H., Hofmann, A.W., Jiang, S.Y., Xu, X.S., 2011. Crust recycling in the sources of two parallel volcanic chains in Shandong, north China. Earth Planet. Sci. Lett. 302, 359–368.
Zeng, G., Chen, L.H., Hu, S.L., Xu, X.S., Yang, L.F., 2013. Genesis of Cenozoic low-Ca alkaline basalts in the Nanjing basaltic field, eastern China: the case for mantle xenolith-magma interaction. Geochem. Geophys. Geosyst. 14, 1660–1677.
Zeng, G., Chen, L.H., Xu, X.S., Jiang, S.Y., Hofmann, A.W., 2010. Carbonated mantle sources for Cenozoic intra-plate alkaline basalts in Shandong, North China. Chem. Geol. 273, 35–45.
Zeng, G., Huang, X.W., Zhou, M.F., Chen, L.H., Xu, X.S., 2016. Using chalcophile elements to constrain crustal contamination and xenolith-magma interaction in Cenozoic basalts of eastern China. Lithos 258–259, 163–172.
Zhang, J.J., Zheng, Y.F., Zhao, Z.F., 2009. Geochemical evidence for interaction between oceanic crust and lithospheric mantle in the origin of Cenozoic continental basalts in east-central China. Lithos 110, 305–326.
Zhang, M., Menzies, M.A., Suddaby, P., Thirlwall, M.F., 1991. EM1 signature from within the post-Archean subcontinental lithospheric mantle: isotopic evidence from the potassium volcanic rocks in NE China. Geochem. J. 25, 387–398.
Zhang, M., Suddaby, P., Thompson, R.N., Thirlwall, M.F., Menzies, M.A., 1995. Potassium volcanic-rocks in NE China: geochemical constraints on mantle source and magma genesis. J. Petrol. 36, 1275–1303.
Zhang, W.H., Han, B.F., 2006. K-Ar chronology and geochemistry of Jining Cenozoic basalts, inner Mongolia, and geodynamic implications. Acta Petrol. Sin. 22, 1597–1607.
Zhang, W.H., Han, B.F., Du, W., Liu, Z.Q., 2005. Characteristics of mantle source for Jining Cenozoic basalts from southern inner Mongolia: evidence from element and Sr-Nd-Pb isotopic geochemistry. Acta Petrol. Sin. 21, 1569–1582.
Zhang, Z.C., Feng, C.Y., Li, Z.N., Li, S.C., Xin, Y., Li, Z.M., Wang, X.Z., 2002. Petrochemical study of the Jingpohu Holocene alkali basaltic rocks, northeastern China. Geochem. J. 36, 133–153.
Zhang, Z.C., Li, Z.N., Li, S.C., Xin, Y., Li, Z.M., Wang, X.Z., 2000. Geochemistry of the Jingpohu Holocene basaltic rocks, Heilongjiang province, and discussion on their deep processes. Acta Petrol. Sin. 16, 327–336.
Zhao, Y.W., Fan, Q.C., Zou, H.B., Li, N., 2014. Geochemistry of Quaternary basaltic lavas from the Nuomin volcanic field, inner Mongolia: implications for the origin of potassium volcanic rocks in northeastern China. Lithos 196–197, 169–180.
Zhi, X.C., Chen, D.G., Yang, J., 1995. Petrogenesis and geochemistry of Neogene basalts in eastern Anhui. Acta Geol. Sin. 8, 406–419.
Zhou, X.H., Molan, E., Zhang, J.B., 1992. Early tertiary basalt in east China sea basin and its implications to regional mantle geochemistry. Acta Petrol. Sin. 8, 395–398 (in Chinese).
Zou, H.B., Fan, Q.C., Yao, Y.P., 2008. U-Th systematics of dispersed young volcanoes in NE China: asthenosphere upwelling caused by piling up and upward thickening of stagnant Pacific slab. Chem. Geol. 255, 134–142.
Zou, H.B., Reid, M.R., Liu, Y.S., Yao, Y.P., Xu, X.S., Fan, Q.C., 2003. Constraints on the origin of historic potassium basalts from northeast China by U-Th disequilibrium data. Chem. Geol. 200, 189–201.
Zou, H.B., Zindler, A., Xu, X.S., Qi, Q., 2000. Major, trace element, and Nd, Sr and Pb isotope studies of Cenozoic basalts in SE China: mantle sources, regional variations, and tectonic significance. Chem. Geol. 171, 33–47.